SIMULATION OF OSMOTIC SWELLING BY THE STOCHASTIC IMMERSED BOUNDARY METHOD[*]

CHEN-HUNG WU[†], THOMAS G. FAI[†], PAUL J. ATZBERGER[‡], AND CHARLES S. PESKIN[†]

Abstract. We develop computational methods for the simulation of osmotic swelling phenomena relevant to microscopic vesicles containing transformable solute molecules. We introduce stochastic immersed boundary methods (SIBMs) that can capture osmotically driven fluid transport through semipermeable elastic membranes subject to thermal fluctuations. We also develop numerical methods to handle within SIBMs an elastic shell model for a neo-Hookean material. Our extended SIBM allows for capturing osmotic swelling phenomena driven by concentration changes and interactions between a discrete collection of confined particles while accounting for the thermal fluctuations of the semipermeable membrane and the hydrodynamic transport of solvent. We use our computational methods to investigate osmotic phenomena in regimes that go beyond the classical Van 't Hoff theory. We develop statistical mechanics theories for osmotic swelling of vesicles when there are significant interactions between particles that can transform over time. We validate our theoretical results against detailed computational simulations. Our methods are expected to be useful for a wide class of applications allowing for the simulation of osmotically driven flows, thermally fluctuating semipermeable elastic structures, and solute interactions.

Key words. osmotic swelling, statistical mechanics, fluid dynamics, thermal fluctuations, fluctuating hydrodynamics, the stochastic immersed boundary method

AMS subject classifications. 65M06, 65C50, 82C80

DOI. 10.1137/14098404X

1. Introduction. Osmotic phenomena play an important role in many biological systems and technological applications [2, 3, 4, 5]. Examples include the manipulation of fluids in microfluidic devices [27, 30, 37] and the transport of nutrients/turgidity in plants [6, 7, 40]. The basic mechanism underlying osmosis involves a concentration difference in the solute particles within a system that often arises from either a semipermeable barrier or an electric field. This allows solvent fluid to cross the barrier but does not allow some species of the solute particles to cross. This results in a chemical potential difference in the system that generates pressures that when out-of-equilibrium can drive elastic deformations of the semipermeable barrier or the transport of solvent fluid.

[†]Courant Institute of Mathematical Sciences, New York University, New York, NY 10012 (chenhung@cims.nyu.edu, tfai@cims.nyu.edu, peskin@courant.nyu.edu). The first author was supported by NYU through the Henry MacCracken Fellowship. The second author was supported by the DOE CSGF fellowship under grant DE-FG02-97ER25308. The fourth author was supported by the Systems Biology Center, New York University, under NIH grant P50-GM071558.

[‡]Department of Mathematics, University of California, Santa Barbara, CA 93106 (atzberg@math.ucsb.edu, http://www.math.ucsb.edu/~atzberg/). This author was supported by the Applied Mathematics Program within the Department of Energy (DOE) Office of Advanced Scientific Computing Research (ASCR) as part of the Collaboratory on Mathematics for Mesoscopic Modeling of Materials (CM4).

The basic theory of osmosis was introduced by Van 't Hoff [8] for the osmotic pressure difference Π between two domains separated by a semipermeable barrier [38]. Van 't Hoff showed that the pressure can be described by $\Pi = \delta c R T$, where R is the ideal gas constant, $\delta c = c_2 - c_1$ is the molar concentration difference between the domains separated by the semipermeable barrier, and T is the temperature of the system in Kelvin. However, the Van 't Hoff theory requires a number of stringent assumptions concerning the solute particles in such a system. These include the following: (i) solute particles are dilute, (ii) solute particles do not interact strongly with one another, and (iii) solute particles interact with the semipermeable barrier as a hard wall with no appreciable interaction length-scale relative to the domain size.

For many biological systems, especially in cell biology, these assumptions are not expected to hold. For example, when proteins or protein assemblies are transported within a cargo vesicle, the confined particles are expected to interact significantly through sterics and electrostatics over an appreciable scale with one another and the vesicle membrane [40]. The Van 't Hoff theory also does not address important questions concerning out-of-equilibrium phenomena that can depend on the transport of solvent driven by osmotic effects, changes in the interactions between solute particles over time, or the role of flexible thermally fluctuating elastic barriers.

In this paper, we introduce a model for osmotic phenomena that can account for hydrodynamic transport of solute, solute particles having significant interactions, and flexible elastic barriers subject to thermal fluctuations. Our work builds on the ideas introduced in the prior works [27, 28] that treat osmotic phenomena in the much more simplified setting of symmetric geometries and impermeable rigid walls. As a motivating application, we develop our model for spherical vesicles that confine a collection of interacting solute particles. We study particular phenomena associated with the osmotic swelling of vesicles that can be driven by the depolymerization of the solute particles that in effect changes the number of confined particles. We show that at equilibrium our mechanical model for osmosis agrees well with the classical Van 't Hoff law. We then perform further investigations and develop a theory for the case when the solute interactions are significant and account for these contributions to the osmotic pressure [28]. We then study through simulations the osmotic swelling of vesicles when the interactions and solute transform over time.

In section 2, we describe the details of our SIBM model and equations of motion for fluid-structure interactions subject to thermal fluctuations based on [21, 24]. We then formulate our model for the mechanics of our elastic membrane taking into account the surface tension, a neo-Hookean shear resistance [32], and Helfrich bending rigidity [22]. We also introduce a potential energy to account for solute particle-particle interactions and membrane-particle interactions.

In section 3, we present numerical methods for the spatial and temporal discretization for the fluid-structure interactions and our elastic shell model for the membrane. We discretize the elastic shell into a triangulated surface and use this representation in our elasticity energy to derive forces in the material coordinates. We use the immersed boundary method kernel introduced by Peskin [1] to couple the Lagrangian and Eulerian coordinates in the fluid-structure interactions.

In section 4, we present simulation results for our model and develop theory. We first validate our model and numerics by simulating the Brownian motion of solute particles diffusing in a spherically symmetric potential. We compare our results with the classical Van 't Hoff's law [9, 10, 11] by a direct computation of the osmotic wall pressure and also by observing the hydrostatic pressure that develops in the fluid. Next, we generalize to the case of a semipermeable vesicle subject to thermal

fluctuations, which deforms in accordance with the elastic energy, and interactions with confined solute particles. We investigate the swelling of the vesicle in size when the solute-solute interactions transform over time (weaken or strengthen). We also develop a statistical mechanics theory for our system based on the solute particle interactions, and we compare our theoretical results with our numerical simulations. We find good agreement between our theory and simulations.

To our knowledge, this work is the first to simulate osmotic swelling of a vesicle incorporating the effects of the elastic membrane, hydrodynamic transport, thermal fluctuations, and, at the particle level, the membrane-solute and solute-solute interactions. Our methods are expected to be useful for a wide class of applications allowing for the simulation of osmotically driven flows, thermally fluctuating semipermeable elastic structures, and, at the particle level, solute-solute interactions.

2. Equations of motion. For mesoscopic systems thermal fluctuations play an important role, giving rise to important entropic contributions to the free energy or contributions in the kinetics such as Brownian motion. We adopt a continuum description of the solvent fluid based on the Navier–Stokes equations that incorporates stochastic fields to account for thermal fluctuations. We consider physical systems where the Reynolds number is rather small [18], allowing us to neglect the nonlinear advection term in the material derivative. However, given the rapid local fluctuations we retain the time derivative term as in the prior works [21, 24, 39]. This leads us to the stochastic time-dependent, incompressible Stokes equations:

$$(2.1) \qquad \rho \frac{\partial \boldsymbol{u}}{\partial t}\left(\boldsymbol{x}, t\right) + \nabla p\left(\boldsymbol{x}, t\right) = \mu \Delta \boldsymbol{u}\left(\boldsymbol{x}, t\right) + \boldsymbol{f}_{\text{total}}\left(\boldsymbol{x}, t\right),$$

$$(2.2) \qquad \nabla \cdot \boldsymbol{u}\left(\boldsymbol{x}, t\right) = 0.$$

Here $\boldsymbol{u}\left(\boldsymbol{x}, t\right)$ denotes the Eulerian velocity field of the fluid at spatial position $\boldsymbol{x} \in \mathcal{G} \subset \mathbb{R}^3$ and time $t \in \mathbb{R}^+$; $p(\boldsymbol{x}, t)$ is the pressure; μ is the uniform dynamic viscosity; ρ is the uniform fluid density; and $\boldsymbol{f}_{\text{total}}\left(\boldsymbol{x}, t\right)$ is the total force density acting on the fluid, including body forces and force densities that arise from thermal fluctuations.

We remark that there has been a lot of work on fluctuating hydrodynamics concerned with both their mathematical structure and their use in physics as a description of mesoscopic phenomena. An analytical study of the Navier–Stokes equations driven by "white noise" was first undertaken by Bensoussan and Temam [12]. Later, this approach was substantially developed and extended by many authors [13, 14, 15, 16, 19, 20, 45, 46]. Computational methods for fluctuating hydrodynamics were developed in [21, 28, 42, 41, 43, 44, 47].

In our work, we use similar fluctuating hydrodynamic descriptions coupled to elastic microstructures by employing the immersed boundary method coupling of [1, 25, 26, 29, 31] and the stochastic Eulerian–Lagrangian method framework of [21]. A significant extension that we introduce here is the ability to capture the dynamics of mechanical structures that are semipermeable to the fluid and the discretization of an elastic shell model for neo-Hookean materials.

We describe the semipermeable membrane as an embedded surface

$$(2.3) \qquad \mathbf{X}_{\text{memb}}\left(\boldsymbol{q}, t\right) \subset \mathbb{R}^3,$$

where $\boldsymbol{q} = (q_1, q_2) \in \mathbb{R}^2$ are material curvilinear coordinates attached to the membrane. The topology of the membrane is that of a sphere. Let Ω be the region contained within this membrane, and let $\partial\Omega$ be the membrane itself.

The elastic energy associated with a fluid phase lipid bilayer membrane was introduced by Helfrich [22] through the bending energy:

$$\mathcal{E}_{\text{bend}}\left[\mathbf{X}_{\text{memb}}\right] = \frac{\kappa_b}{2}\int_{\partial\Omega} H^2 dA, \tag{2.4}$$

where κ_b is the bending modulus, dA is the element of area, and H is twice the mean curvature; i.e., H is the sum of the two principal curvatures at any point of the membrane.

In addition to the bending energy, we consider a membrane that resists both stretch and shear in an elastic manner. For the energy associated with changes in the area of any part of the membrane, we introduce the surface tension energy

$$\mathcal{E}_{\text{tension}}\left[\mathbf{X}_{\text{memb}}\right] = \sigma\int_{\partial\Omega} dA, \tag{2.5}$$

where σ is a constant equal to the surface tension at every point of the membrane, and dA is the element of area on $\partial\Omega$. This is the kind of surface tension that we use throughout this paper. We remark that this is unrealistic for a lipid bilayer, which resists local changes in area much more strongly. The reason that we use a simple surface tension model is so that we can easily see osmotic swelling as a change in size of the vesicle, and not merely as a change in shape or as a rise in pressure.

A more realistic model for the stretch resistance of the vesicle that could be considered is

$$\mathcal{E}_{\text{tension}}\left[\mathbf{X}_{\text{memb}}\right] = \sigma\int_{\partial\Omega_0} \left|\frac{dA - dA_0}{dA_0}\right|^m dA_0, \tag{2.6}$$

where m is a parameter that controls the sensitivity of the surface-tension energy to local changes in membrane area, $\partial\Omega_0$ is the reference configuration of the membrane, dA_0 is the area element of the reference configuration, and dA is the area element of the deformed configuration. Strictly speaking, even when $m = 1$, (2.6) does not reduce to (2.5) because of the absolute value in (2.6). However, if $m = 1$ and $dA > dA_0$ everywhere, then (2.5) and (2.6) are effectively the same since the absolute value becomes irrelevant and the extra term in (2.6) becomes constant. We do not use (2.6) in this paper, however, and mention it here only as a generalization that would be considered in the future.

Besides curvature and stretch, our model membrane also resists shear. This is modeled using a two-dimensional neo-Hookean energy (without any bulk term). Let $\mathbf{Z}\left(\boldsymbol{q}\right) \in \mathbb{R}^3$ be the reference configuration, and let $\mathbf{X}_{\text{memb}}\left(\boldsymbol{q}, t\right)$ be the corresponding deformed configuration at time t. Then $\partial\mathbf{X}_{\text{memb}}/\partial\boldsymbol{q}$ and $\partial\mathbf{Z}/\partial\boldsymbol{q}$ are 3×2 matrices, and right Cauchy–Green deformation tensors are defined by

$$\mathbb{G} = \left(\frac{\partial\mathbf{X}_{\text{memb}}}{\partial\boldsymbol{q}}\right)^T \left(\frac{\partial\mathbf{X}_{\text{memb}}}{\partial\boldsymbol{q}}\right), \tag{2.7}$$

$$\mathbb{G}_0 = \left(\frac{\partial\mathbf{Z}}{\partial\boldsymbol{q}}\right)^T \left(\frac{\partial\mathbf{Z}}{\partial\boldsymbol{q}}\right) \tag{2.8}$$

and are 2×2, symmetric, and positive definite matrices. Notice that the "row vector" convention is adopted for the vector-valued derivative in (2.7). The two-dimensional neo-Hookean shear potential is

$$\mathcal{E}_{\text{shear}}\left[\mathbf{X}_{\text{memb}}\right] = \frac{\kappa_s}{2}\int \left(\text{trace}\left(\mathbb{G}\mathbb{G}_0^{-1}\right)\left(\frac{\det\mathbb{G}}{\det\mathbb{G}_0}\right)^{-\frac{1}{2}} - 2\right)\left(\det\mathbb{G}_0\right)^{\frac{1}{2}} d\boldsymbol{q}, \tag{2.9}$$

where κ_s is the shear modulus of the membrane.

Although we use (2.9) directly for computational purposes (see Appendix A.3 in the supplementary material), the meaning of (2.9) is clarified by rewriting it in terms of the principal stretches λ_1 and λ_2, which are positive numbers such that λ_1^2 and λ_2^2 are the eigenvalues of $\mathbb{G}\mathbb{G}_0^{-1}$. The expression for $\mathcal{E}_{\text{shear}}$ in terms of λ_1 and λ_2 is

$$(2.10) \qquad \mathcal{E}_{\text{shear}}\left[\mathbf{X}_{\text{memb}}\right] = \frac{\kappa_s}{2} \int \left(\frac{\lambda_1^2 + \lambda_2^2}{\lambda_1 \lambda_2} - 2 \right) \left(\det \mathbb{G}_0 \right)^{\frac{1}{2}} d\boldsymbol{q}.$$

The above formulation of a neo-Hookean surface shear energy differs from that of a three-dimensional neo-Hookean material in two important ways. The constant -2 that appears (2.9) would be -3 in the case of a three-dimensional material, and the exponent $-1/2$ that appears (2.9) would be $-2/3$. Our choices of these constants have the effect that $\mathcal{E}_{\text{shear}}$ is invariant under a change of scale. That is, with the reference configuration held fixed,

$$(2.11) \qquad \mathcal{E}_{\text{shear}}\left(r\mathbf{X}\right) = \mathcal{E}_{\text{shear}}\left(\mathbf{X}\right)$$

for any configuration $\mathbf{X}$ and any positive constant r. Since the Helfrich bending energy is also scale-invariant, the only term in the membrane energy that resists osmotic swelling is the surface tension.

In addition to the elastic potentials of the membrane, we consider the osmotic effect of N_p identical and possibly interacting solute particles $\mathbf{X}_{\text{prt}}^{(k)}$ contained by the membrane vesicle $\mathbf{X}_{\text{memb}}$. For each solute particle we take into account the particle-membrane interaction potential

$$(2.12) \qquad \Theta \left(\left\| \mathbf{X}_{\text{prt}}^{(k)} - \mathbf{X}_{\text{memb}}(\boldsymbol{q}) \right\| \right)$$

and the particle-particle interaction potential

$$(2.13) \qquad \Psi_{k,j} \left(\left\| \mathbf{X}_{\text{prt}}^{(k)} - \mathbf{X}_{\text{prt}}^{(j)} \right\| \right),$$

where $\|\cdot\|$ denotes the Euclidean norm. In what follows, the total interaction potential is given by

$$(2.14) \quad \Phi\left(\mathbf{X}\right) = \int \sum_{k=1}^{N_p} \Theta \left(\left\| \mathbf{X}_{\text{prt}}^{(k)} - \mathbf{X}_{\text{memb}}\left(\boldsymbol{q}\right) \right\| \right) d\boldsymbol{q} + \sum_{\substack{k,j=1 \\ k<j}}^{N_p} \Psi_{k,j} \left(\left\| \mathbf{X}_{\text{prt}}^{(k)} - \mathbf{X}_{\text{prt}}^{(j)} \right\| \right),$$

with

$$(2.15) \qquad \mathbf{X} := \left(\mathbf{X}_{\text{memb}}, \mathbf{X}_{\text{prt}}^{(1)}, \ldots, \mathbf{X}_{\text{prt}}^{(N_p)} \right),$$

so that $\mathbf{X}$ gives the combined configuration of the membrane and the solute particles.

We combine the four potentials from (2.4), (2.5), and (2.10), and let

$$(2.16) \quad \mathcal{E}\left[\mathbf{X}\right] = \mathcal{E}_{\text{bend}}\left[\mathbf{X}_{\text{memb}}\right] + \mathcal{E}_{\text{tension}}\left[\mathbf{X}_{\text{memb}}\right] + \mathcal{E}_{\text{shear}}\left[\mathbf{X}_{\text{memb}}\right] + \Phi\left[\mathbf{X}_{\text{memb}}, \mathbf{X}_{\text{prt}}\right]$$

be the total potential energy of the system, including both the elastic energy of the vesicle membrane and also the solute-membrane and solute-solute interaction potentials.

The membrane-solute system described above is immersed in a thermally fluctuating fluid. To model this, we use the methodology described in [21], specifically regime II of the stochastic Eulerian–Lagrangian method (SELM), which assumes that the immersed materials (membrane and solute) are neutrally buoyant and that their interactions with the ambient fluid are overdamped. We use this formulation and adjust the drag operator so that the immersed material can slip relative to the surrounding fluid. We use this to model the permeability of the membrane to the fluid. This feature is essential for us to allow for the osmotic swelling to occur by the in-flux or out-flux of fluid through the membrane.

Two types of random forces are used. A Lagrangian random force is applied directly to the immersed material to achieve fluctuation-dissipation balance with the slip resistance. An Eulerian random force is applied to the fluid to achieve fluctuation-dissipation balance with the fluid shear viscosity. Together, these random forces bring the system to thermal equilibrium at a specified temperature T.

The governing equations are as follows. For the fluid, we have the time-dependent Stokes equations (2.1)–(2.2), in which

$$(2.17) \qquad \boldsymbol{f}_{\text{total}}(\boldsymbol{x}, t) = \Lambda \mathbf{F} + (\nabla_{\mathbf{X}} \cdot \Lambda) k_{\text{B}} T + \boldsymbol{g}_{\text{thm}},$$

and for the immersed material we have the overdamped equation of motion

$$(2.18) \qquad \frac{\partial \mathbf{X}}{\partial t} = \Gamma \boldsymbol{u}(\boldsymbol{x}, t) + \Upsilon^{-1} (\mathbf{F} + \mathbf{F}_{\text{thm}}).$$

Here T is the absolute temperature in degrees Kelvin, k_{B} is the Boltzmann constant, and Υ is a positive definite dissipative operator describing the viscous interactions coupling the structure to the fluid. Along with Υ, the other two operators Γ and Λ in (2.17) and (2.18) will be defined later.

In these equations, the force density $\mathbf{F}$ is the variational derivative of the elastic energy functional $\mathcal{E}[\mathbf{X}]$:

$$(2.19) \qquad \mathbf{F} = -\frac{\boldsymbol{\delta} \mathcal{E}[\mathbf{X}]}{\boldsymbol{\delta} \mathbf{X}}.$$

Here we use $\boldsymbol{\delta}$ instead of the more conventional symbol δ to avoid confusion with the kernel function, which appears later. We point out here that (2.19) has both a continuous and a discrete part:

$$(2.20) \qquad \mathbf{F} = \left(\mathbf{F}_{\text{memb}}(\boldsymbol{q}), \mathbf{F}_{\text{prt}}^{(1)}, \mathbf{F}_{\text{prt}}^{(2)}, \dots, \mathbf{F}_{\text{prt}}^{(N_p)} \right).$$

The meaning of (2.19) is that, to first order in $\boldsymbol{\delta} \mathbf{X}$,

$$(2.21) \qquad \boldsymbol{\delta} \mathcal{E} = -\int \mathbf{F}_{\text{memb}}(\boldsymbol{q}) \cdot \boldsymbol{\delta} \mathbf{X}_{\text{memb}}(\boldsymbol{q}) \, d\boldsymbol{q} - \sum_{k=1}^{N_p} \mathbf{F}_{\text{prt}}^{(k)} \cdot \boldsymbol{\delta} \mathbf{X}_{\text{prt}}^{(k)}.$$

Note in particular that $\mathbf{F}_{\text{memb}}$ is a force density with respect to the Lebesgue measure $d\boldsymbol{q}$, but that $\mathbf{F}_{\text{prt}}$ is a *force*, not a force density.

The force density $\mathbf{F}_{\text{memb}}$ applied by the membrane to the surrounding fluid is

$$(2.22) \qquad \mathbf{F}_{\text{memb}} = -\frac{\boldsymbol{\delta} \mathcal{E}[\mathbf{X}]}{\boldsymbol{\delta} \mathbf{X}_{\text{memb}}},$$

and the force acting on the kth solute particle and transmitted by that particle to the fluid is

$$(2.23) \qquad \mathbf{F}_{\mathrm{prt}}^{(k)} = -\frac{\partial \mathcal{E}\left[\mathbf{X}\right]}{\partial \mathbf{X}_k} = -\frac{\partial \Phi\left(\mathbf{X}\right)}{\partial \mathbf{X}_k}.$$

In (2.23), we are using the notation of a partial derivative with respect to a vector. Thus, in components,

$$(2.24) \qquad F_{\mathrm{prt},\alpha}^{(k)} = -\frac{\partial \mathcal{E}\left[\mathbf{X}\right]}{\partial X_{k,\alpha}}$$

for $\alpha = 1, 2, 3$.

The stochastic driving fields (random forces) are taken to be Gaussian random fields that are white noise in time with zero mean and spatial covariance structure given by the fluctuation-dissipation principle [21]:

$$(2.25) \qquad \left\langle \mathbf{F}_{\mathrm{thm}}(\boldsymbol{q},s)\mathbf{F}_{\mathrm{thm}}^{\mathrm{T}}(\boldsymbol{q}',t)\right\rangle = 2k_{\mathrm{B}}T\Upsilon\delta(t-s)\delta(\boldsymbol{q}-\boldsymbol{q}'),$$

$$(2.26) \qquad \left\langle \boldsymbol{g}_{\mathrm{thm}}(\boldsymbol{x},s)\boldsymbol{g}_{\mathrm{thm}}^{\mathrm{T}}(\boldsymbol{x}',t)\right\rangle = -2k_{\mathrm{B}}T\mu\Delta\delta(t-s)\delta(\boldsymbol{x}-\boldsymbol{x}'),$$

$$(2.27) \qquad \left\langle \mathbf{F}_{\mathrm{thm}}(\boldsymbol{q},s)\boldsymbol{g}_{\mathrm{thm}}^{\mathrm{T}}(\boldsymbol{x},t)\right\rangle = 0,$$

where Δ is the vector Laplacian.

In this paper, we construct Υ as a block diagonal matrix with 3×3 blocks by assigning a scalar γ_k to each Lagrangian point in the simulation and then setting the kth diagonal block of Υ equal to $\gamma_k\mathbf{I}$, where $\mathbf{I}$ is the 3×3 identity matrix. For solute particles, the value of γ_k is given by the Stokes drag formula

$$(2.28) \qquad \gamma_k = 6\pi\mu r_k,$$

where μ is the viscosity of the fluid and r_k is the Stokes radius of the solute particle.

In our model, the slip-coefficient γ_k^{-1} in (2.18) accounts for the permeability to fluid of a patch of the membrane. Our model accounts for the passage of fluid through the membrane by allowing for "slip" of the control points representing the membrane relative to the local fluid velocity. Our model is an analogue of Darcy's law where at steady state our membrane velocity is proportional to the normal component of the local "pressure" acting on the membrane. In our model this pressure (force per unit area) is determined from $\mathbf{F} + \mathbf{F}_{\mathrm{thm}}$.

Because we have chosen to make all of the diagonal blocks of Υ be multiples of the identity, we get tangential as well as normal slip between the membrane and the fluid. The tangential slip could be avoided by making the kth diagonal block of Υ^{-1} be of the form $\gamma_k^{-1}\mathbf{n}_k\mathbf{n}_k^T$, where $\mathbf{n}_k$ is the unit normal to the membrane at the membrane point k, and the superscript T denotes matrix transposition, so that $\mathbf{n}_k\mathbf{n}_k^T$ is a 3×3, rank-1 matrix, but we avoid this complication for now.

To convert between Lagrangian and Eulerian coordinates, we introduce two linear conjugate operators [1, 21]: Λ, a spreading operator defined by

$$(2.29) \qquad \begin{aligned}(\Lambda\mathbf{F})(\boldsymbol{x},t) &= \int_\Omega \mathbf{F}_{\mathrm{memb}}(\boldsymbol{q},t)\,\delta_c\left(\boldsymbol{x}-\mathbf{X}(\boldsymbol{q},t)\right)d\boldsymbol{q} \\ &+ \sum_{k=1}^{N_p}\mathbf{F}_{\mathrm{prt}}^{(k)}(t)\,\delta_c\left(\boldsymbol{x}-\mathbf{X}_{\mathrm{prt}}^{(k)}(t)\right),\end{aligned}$$

and, similarly, the local averaging operator Γ, denoted by Γ_{memb} and Γ_{prt} for membrane and solute particles, respectively:

$$(2.30) \quad (\Gamma_{\mathrm{memb}}\boldsymbol{u})\,(\boldsymbol{q},t) = \int \boldsymbol{u}\,(\boldsymbol{x},t)\,\delta_c\,(\boldsymbol{x} - \mathbf{X}\,(\boldsymbol{q},t))\,d\boldsymbol{x}, \qquad \boldsymbol{q} \in \Omega,$$

$$(2.31) \quad (\Gamma_{\mathrm{prt}}\boldsymbol{u})_k\,(t) = \int \boldsymbol{u}\,(\boldsymbol{x},t)\,\delta_c\left(\boldsymbol{x} - \mathbf{X}_{\mathrm{prt}}^{(k)}\,(t)\right)d\boldsymbol{x}, \qquad k \in \{1\ldots N_p\},$$

for arbitrary functions $\mathbf{F}$ and $\boldsymbol{u}$. These operators both involve a three-dimensional kernel function $\delta_c(\boldsymbol{r})$ similar to the one in the discussion in [1, 21]. This function will be defined below.

We remark that there are two primary reasons that we introduce a kernel function (as opposed to a Dirac δ-function) in our continuum mechanics description of the system. The first reason has to do with calibrating the mobility M of a particle represented in the immersed boundary method by the operators that perform the force-spreading Λ and velocity-averaging Γ. The mobility M gives the steady-state velocity $\mathbf{V}$ in response to an applied force $\mathbf{F}$ by $\mathbf{V} = M\mathbf{F}$. The operators Γ, Λ have been shown to be related to an immersed boundary particle's mobility by $M = \Gamma\mathcal{L}^{-1}\Lambda$. The $\mathcal{L}^{-1}$ denotes the solution operator for the fluid velocity $\mathbf{u}$ of the steady-state incompressible Stokes equations with force density $\mathbf{f} = \Lambda\mathbf{F}$; see [21, 24]. An important result is that the particle mobility satisfies $\mathbf{V} = M\mathbf{F} = \Gamma\mathbf{u}$ for the force density $\mathbf{f}$. If the Dirac δ-function ($c = 0$) is used for the operators, the force density is a Dirac δ-function and generates in the Stokes flow a singular velocity field $\mathbf{u}$ at the particle location. The Γ operator then involves a Dirac δ-function ($c = 0$) and results in evaluating the velocity field at the particle location which is singular. As a consequence, a model of a single particle must use an operator Λ that spreads the force over a finite length-scale $c > 0$. To calibrate the immersed boundary particle mobility M we use the kernel function δ_c and introduce the length-scale c, which is closely related to the particle's hydrodynamic radius.

The second reason we use a kernel function δ_c has to do with the behavior of fluctuating hydrodynamics. In the continuum description the thermal fluctuations are modeled by a stochastic driving field that is Dirac δ-correlated in space. As a consequence, the fluctuating hydrodynamic equations generate a fluid velocity $\mathbf{u}$ that is a generalized function (distribution) which is not defined pointwise. When modeling the diffusion of material points the operator Γ cannot simply evaluate the fluid velocity $\mathbf{u}$ at the particle location but instead must perform an average over some nonzero length-scale. Similar to the mobility calculations, to obtain a finite diffusivity for the particles and membrane we introduce the kernel function δ_c and length-scale c, which for isolated particles is closely related to the particle's hydrodynamic radius. More discussion can be found in [21, 24].

The operators Λ and Γ are adjoint in the following sense:

$$(2.32) \qquad \int_\Omega (\Gamma\varphi)\,(\boldsymbol{q}) \cdot \psi\,(\boldsymbol{q})\;d\boldsymbol{q} = \int_\mathcal{G} \varphi\,(\boldsymbol{x}) \cdot (\Lambda\psi)\,(\boldsymbol{x})\;d\boldsymbol{x}$$

for all smooth functions φ and ψ, where the domains of the structures and the fluid are denoted by Ω and $\mathcal{G}$, respectively. This ensures a form of conservation of energy in the Eulerian–Lagrangian coupling, in the sense that the rate at which the immersed boundary does work in the fluid comes out the same, regardless of whether it is expressed in terms of Lagrangian or Eulerian variables.

The operator Λ also appears in (2.17) through the term $(\nabla_{\mathbf{X}} \cdot \Lambda) k_{\mathrm{B}} T$. This describes a deterministic drift induced by the fluctuations that vary with the configuration of the immersed structure. This arises from the Itô calculus formulation of the stochastic PDEs and is explained in [21], and its implementation here is described below (see (3.32)). In summary, the complete structure-fluid coupled system of equations is given by

$$\rho \frac{\partial \boldsymbol{u}}{\partial t} (\boldsymbol{x}, t) + \nabla p (\boldsymbol{x}, t) = \mu \Delta \boldsymbol{u} (\boldsymbol{x}, t) + \boldsymbol{f}_{\mathrm{total}} (\boldsymbol{x}, t), \tag{2.33}$$

$$\nabla \cdot \boldsymbol{u} (\boldsymbol{x}, t) = 0, \tag{2.34}$$

$$\mathcal{E} [\mathbf{X}] = \mathcal{E}_{\mathrm{bend}} [\mathbf{X}_{\mathrm{memb}}] + \mathcal{E}_{\mathrm{tension}} [\mathbf{X}_{\mathrm{memb}}]$$
$$+ \mathcal{E}_{\mathrm{shear}} [\mathbf{X}_{\mathrm{memb}}] + \Phi (\mathbf{X}), \tag{2.35}$$

$$\mathbf{F}_{\mathrm{memb}} = -\frac{\boldsymbol{\delta} \mathcal{E} [\mathbf{X}]}{\boldsymbol{\delta} \mathbf{X}_{\mathrm{memb}}}, \tag{2.36}$$

$$\mathbf{F}_{\mathrm{prt}}^{(k)} = -\frac{\partial \mathcal{E} [\mathbf{X}]}{\partial \mathbf{X}_k} = -\frac{\partial \Phi (\mathbf{X})}{\partial \mathbf{X}_k}, \tag{2.37}$$

$$\boldsymbol{f}_{\mathrm{total}} (\boldsymbol{x}, t) = \Lambda \mathbf{F} + (\nabla_{\mathbf{X}} \cdot \Lambda) k_{\mathrm{B}} T + \boldsymbol{g}_{\mathrm{thm}}, \tag{2.38}$$

$$\frac{\partial \mathbf{X}}{\partial t} = \Gamma \boldsymbol{u} (\boldsymbol{x}, t) + \Upsilon^{-1} (\mathbf{F} + \mathbf{F}_{\mathrm{thm}}). \tag{2.39}$$

3. Numerical method. In this section, we discuss the discretizations of (2.33)–(2.39). First, in section 3.1, we discuss the three different elastic membrane energies. Subsequently, in section 3.2, by introducing a particular kernel function, we specify the coupling between the Lagrangian and Eulerian variables. The interaction potential is discussed in section 3.3. The spatial discretization of (2.33)–(2.39) is given in section 3.4, followed by the temporal discretization in section 3.5.

3.1. Discretization of membrane potentials and evaluation of the corresponding forces. Given a deformed configuration $\mathbf{X}_{\mathrm{memb}} (t)$ at time t, we present the discretizations of the bending, tension, and neo-Hookean potentials. We discretize the membrane vesicle by a triangular mesh with N_ν vertices:

$$\mathbf{X}_{\mathrm{memb}}^{(1)} (t), \mathbf{X}_{\mathrm{memb}}^{(2)} (t), \ldots, \mathbf{X}_{\mathrm{memb}}^{(N_\nu)} (t). \tag{3.1}$$

The discretized elastic energy functional will then be a function of the form

$$\widetilde{\mathcal{E}_{\mathcal{I}}} [\mathbf{X}_{\mathrm{memb}} (t)] = \widetilde{\mathcal{E}_{\mathcal{I}}} \left[\mathbf{X}_{\mathrm{memb}}^{(1)} (t), \mathbf{X}_{\mathrm{memb}}^{(2)} (t), \ldots, \mathbf{X}_{\mathrm{memb}}^{(N_\nu)} (t) \right] \tag{3.2}$$

for the subscripted index $\mathcal{I} = $ *bend, tension,* or *shear*. The specific function we use in each case is described in Appendix A in the supplementary material. The parenthesized superscripts index the vertices of the discretized membrane, and the tilde symbol stands for the discretized approximation to the elastic energy. As we refine the discretization of the vesicle, that is, as $N_\nu \to \infty$, $\widetilde{\mathcal{E}_{\mathcal{I}}}$ approaches $\mathcal{E}_{\mathcal{I}}$. From now on, we consider the time-dependence to be understood and write $\mathbf{X}_{\mathrm{memb}} (t) = \mathbf{X}_{\mathrm{memb}}$.

Recall that in (2.36), the first variational derivative of the elastic energy functional is minus the Lagrangian force density. We define the analogous discrete quantity by taking the gradient of the elastic energy: $\nabla_{\mathbf{X}} \widetilde{\mathcal{E}_{\mathcal{I}}}$. Consequently, the force at the kth node becomes

$$\mathbf{F}^{(k)} = -\frac{\partial \widetilde{\mathcal{E}_{\mathcal{I}}} [\mathbf{X}_{\mathrm{memb}}]}{\partial \mathbf{X}_{\mathrm{memb}}^{(k)}} \tag{3.3}$$

for $k = 1, \ldots, N_\nu$. Recall that we are using the notation that the partial derivative with respect to a vector denotes the gradient with respect to that vector. That is, in components,

$$(3.4) \qquad F_\alpha^{(k)} = -\frac{\partial \widetilde{\mathcal{E}_\mathcal{I}}\left[\mathbf{X}_{\text{memb}}\right]}{\partial \left(X_{\text{memb}}^{(k)}\right)_\alpha}$$

for $\alpha = 1, 2, 3$.

It is worth pointing out that as we refine the triangular mesh, i.e., in the limit that the mesh width goes to zero or as the number of the vesicle markers $N_\nu \to \infty$, $\mathbf{F}^{(k)} \to 0$. The reason is that $\mathbf{F}^{(k)}$ is the force, rather than the force density. On the other hand,

$$(3.5) \qquad \lim_{N_\nu \to \infty} \sum_{\substack{k=1 \\ k:\mathbf{X}_k \in V}}^{N_\nu} \mathbf{F}^{(k)} = \mathbf{F}(\mathcal{V}),$$

where $\mathcal{V}$ is any sufficiently regular subset of $\mathbb{R}^3$. Here, $\mathbf{F}(\mathcal{V})$ is finite and typically nonzero if $\mathcal{V}$ contains any point of the vesicle membrane, and has the interpretation of being the total force applied to the fluid by the part of the vesicle membrane that lies within $\mathcal{V}$. For the details of the force computation, see Appendix A in the supplementary material.

3.2. Interaction kernel. Once we find the Lagrangian forces from the elastic energy as described above, the next question is how to compute the force density in Eulerian coordinates. For this purpose, we introduce an interaction kernel function. This same kernel function will also be used later for velocity interpolation.

We use the interaction kernel of width $4c$ described in [1]. It is defined as follows: for any $\boldsymbol{r} = (r_1, r_2, r_3) \in \mathbb{R}^3$,

$$(3.6) \qquad \delta_c\left(\boldsymbol{r}\right) := \frac{1}{c^3}\varphi\left(\frac{r_1}{c}\right)\varphi\left(\frac{r_2}{c}\right)\varphi\left(\frac{r_3}{c}\right),$$

where $\varphi\left(r\right)$ is compactly supported (its support has width 4) and is defined piecewise by

$$(3.7) \qquad \varphi(r) = \begin{cases} \frac{1}{8}\left(3 - 2\left|r\right| + \sqrt{1 + 4\left|r\right| - 4\left|r\right|^2}\right) & \text{for } 0 \leq \left|r\right| \leq 1, \\ \frac{1}{8}\left(5 - 2\left|r\right| - \sqrt{-7 + 12\left|r\right| - 4\left|r\right|^2}\right) & \text{for } 1 \leq \left|r\right| \leq 2, \\ 0 & \text{for } \left|r\right| > 2. \end{cases}$$

The derivation of this kernel from a collection of properties that one would like an interaction kernel function to have is described in [1]. For completeness, we also include the analytic derivative of φ that is used to find the force density of the wall-solute interaction potential:

$$(3.8) \qquad \varphi'(r) = \begin{cases} \frac{\text{sgn}(r)}{4}\left(-1 + \frac{1 - 2\left|r\right|}{\sqrt{1 + 4\left|r\right| - 4r^2}}\right) & \text{for } 0 \leq \left|r\right| \leq 1, \\ \frac{\text{sgn}(r)}{4}\left(-1 - \frac{3 - 2\left|r\right|}{\sqrt{-7 + 12\left|r\right| - 4r^2}}\right) & \text{for } 1 \leq \left|r\right| \leq 2, \\ 0 & \text{for } \left|r\right| > 2. \end{cases}$$

Note that $\varphi(r)$ and $\varphi'(r)$ are both continuous functions.

We remark that as the grid is refined, one should hold c constant as $h \to 0$. However, in practice, one often finds in a typical immersed boundary simulation that $c \sim h$. This arises since the parameter c is comparable to the particle's hydrodynamic radius and serves to determine the mobility of an immersed particle. On the other hand, the mesh width h used in numerical discretizations is often employed for computational efficiency to be on the order of the smallest relevant features in the fluid flow. Since these two length-scales are comparable, this results in the use of the grid refinement $h \sim c$. During grid refinements c should be held fixed to retain the particle mobility. A best practice to benefit from the numerical advantages of the Peskin kernel function [1] is to choose a mesh width so that c is an integer multiple of h.

3.3. Interaction potential. In this section, we describe the discretization of the interaction potential $\Phi(\mathbf{X})$ that is defined in (2.14) above. Also we specify the functions Θ and $\Psi_{k,j}$ from which that interaction potential is constructed, and we give expressions for the forces that are derived from the interaction potential.

The discretization is accomplished simply by replacing the integral in (2.14) by a sum

$$(3.9) \quad \tilde{\Phi}\left(\mathbf{X}\right) = \sum_{\ell=1}^{N_\nu} \sum_{k=1}^{N_p} \Theta\left(\left\|\mathbf{X}_{\mathrm{prt}}^{(k)} - \mathbf{X}_{\mathrm{memb}}^{(\ell)}\right\|\right) \Delta\boldsymbol{q} + \sum_{\substack{k,j=1 \\ k<j}}^{N_p} \Psi_{k,j}\left(\left\|\mathbf{X}_{\mathrm{prt}}^{(k)} - \mathbf{X}_{\mathrm{prt}}^{(j)}\right\|\right),$$

where

$$(3.10) \qquad\qquad \mathbf{X} = \left(\mathbf{X}_{\mathrm{memb}}^{(1)}, \dots, \mathbf{X}_{\mathrm{memb}}^{(N_\nu)}, \mathbf{X}_{\mathrm{prt}}^{(1)}, \dots, \mathbf{X}_{\mathrm{prt}}^{(N_p)}\right),$$

and where N_p is the number of solute particles, N_ν is the number of Lagrangian points representing the vesicle membrane, and $\Delta\boldsymbol{q}$ is the Lagrangian measure assigned to each membrane point, so that $N_\nu\Delta\boldsymbol{q}$ is the total Lagrangian measure of the vesicle membrane.

The function Θ can be any bell-shaped function of one variable. The argument of Θ is the distance R between a point on the vesicle membrane and a solute particle. For computational efficiency, Θ should have finite range, i.e., bounded support. Since we already have such a function available, we use a scaled version of the one-dimensional kernel function for this purpose. Thus, we use

$$(3.11) \qquad\qquad \Theta\left(R\right) = \lambda\delta_c\left(R\right) = \frac{\lambda}{c}\varphi\left(\frac{R}{c}\right),$$

where φ is defined by (3.7), and λ is a scaling parameter chosen to make a potential barrier that is large enough to prevent solute particles from crossing the vesicle membrane. The distance $4c$ can be thought of as the effective "thickness" of the membrane in our model; see Figure 1.

The function Ψ is needed only for applications involving solutes with internal structure, so that each solute molecule needs to be represented by more than one particle. The only example of this that occurs in the present paper is a collection of dimers. To describe such a collection, let $\mathcal{D}$ be the set of ordered pairs (k,j) such that $k<j$ and particles k and j belong to the same dimer. Then $N_p = 2\left|\mathcal{D}\right|$, and

$$(3.12) \qquad\qquad \Psi_{k,j}\left(R\right) = \begin{cases} \frac{1}{2}KR^2, & (k,j) \in \mathcal{D}, \\ 0 & \text{otherwise}, \end{cases}$$

FIG. 1. *The thin shell around the boundary represents where solute particles interact with the vesicle wall. A wall-particle interaction potential Θ is chosen such that the energy barrier is approximately $15k_\mathrm{B}T$ to avoid significant leakage, that is, to ensure that the particles stay inside the vesicle.*

where K is a constant with units of force/length that gives the stiffness of each dimer. (We are assuming here that all of the dimers are identical.) In applications involving monomers only, the terms involving Ψ in (3.9) are not used at all.

The forces that result from $\tilde{\Phi}$ are as follows:

$$
\begin{aligned}
\mathbf{F}_{\mathrm{prt}}^{(k)} &= -\frac{\partial \tilde{\Phi}}{\partial \mathbf{X}_{\mathrm{prt}}^{(k)}} \\
&= \sum_{\ell=1}^{N_\nu} \Theta'\left(\left\|\mathbf{X}_{\mathrm{prt}}^{(k)} - \mathbf{X}_{\mathrm{memb}}^{(\ell)}\right\|\right) \frac{\mathbf{X}_{\mathrm{memb}}^{(\ell)} - \mathbf{X}_{\mathrm{prt}}^{(k)}}{\left\|\mathbf{X}_{\mathrm{memb}}^{(\ell)} - \mathbf{X}_{\mathrm{prt}}^{(k)}\right\|} \Delta \boldsymbol{q} \\
&\quad + \sum_{\substack{j=1 \\ j \neq k}}^{N_p} \Psi'_{k,j}\left(\left\|\mathbf{X}_{\mathrm{prt}}^{(k)} - \mathbf{X}_{\mathrm{prt}}^{(j)}\right\|\right) \frac{\mathbf{X}_{\mathrm{prt}}^{(j)} - \mathbf{X}_{\mathrm{prt}}^{(k)}}{\left\|\mathbf{X}_{\mathrm{prt}}^{(j)} - \mathbf{X}_{\mathrm{prt}}^{(k)}\right\|},
\end{aligned}
\tag{3.13}
$$

$$
\begin{aligned}
\mathbf{F}_{\mathrm{memb}}^{(\ell)} &= -\frac{\partial \tilde{\Phi}}{\partial \mathbf{X}_{\mathrm{memb}}^{(\ell)}} \\
&= \sum_{\ell=1}^{N_p} \Theta'\left(\left\|\mathbf{X}_{\mathrm{prt}}^{(k)} - \mathbf{X}_{\mathrm{memb}}^{(\ell)}\right\|\right) \frac{\mathbf{X}_{\mathrm{prt}}^{(k)} - \mathbf{X}_{\mathrm{memb}}^{(\ell)}}{\left\|\mathbf{X}_{\mathrm{prt}}^{(k)} - \mathbf{X}_{\mathrm{memb}}^{(\ell)}\right\|} \Delta \boldsymbol{q},
\end{aligned}
\tag{3.14}
$$

where $f'(x)$ denotes the derivative of any function of one variable $f(x)$.

In the special case that the solute molecules are monomers, the term involving Ψ in (3.13) is zero, and in the special case of dimers, the whole sum involving Ψ reduces to the single term

$$
K\left(\mathbf{X}_{\mathrm{prt}}^{(j(k))} - \mathbf{X}_{\mathrm{prt}}^{(k)}\right),
\tag{3.15}
$$

where $j(k)$ is the index of the particle that is linked to particle k to form a dimer.

Note that the $\mathbf{F}_{\mathrm{prt}}^{(k)}$ and the $\mathbf{F}_{\mathrm{memb}}^{(\ell)}$ are forces, not force densities. Also, as $\Delta \boldsymbol{q} \to 0$, $\mathbf{F}_{\mathrm{prt}}^{(k)} = \mathcal{O}(1)$, since $N_\nu \Delta \boldsymbol{q} = \mathcal{O}(1)$, but $\mathbf{F}_{\mathrm{memb}}^{(\ell)} = \mathcal{O}(\Delta \boldsymbol{q})$, since $N_p \Delta q = \mathcal{O}(\Delta \boldsymbol{q})$.

Finally, for completeness, we note that

$$(3.16) \qquad \Theta'(R) = \frac{\lambda}{c^2} \varphi'\left(\frac{R}{c}\right),$$

and that φ' is given by (3.8).

We remark that in principle the total number of operations required to compute the particle-membrane forces is $\mathcal{O}(N_\nu N_p)$. It should be mentioned that this cost can be reduced by taking advantage of the finite range of the interaction, which we have denoted by the parameter c. For the range of N_p encountered in our models in the present work, we have found that the fluid calculations dominate the computational cost at each time step. However, for other models this may not be the case, and we mention briefly a way the particle-interaction costs can be reduced. This can be done by introducing a cubic lattice of cells of width $2c$ and sorting the membrane points and the solute particles according to the cells in which they lie at any given time step. Since each solute particle or membrane point can be classified based on its coordinates alone, the work to do this sorting is $\mathcal{O}(N_\nu + N_p)$. Now a given solute particle in a particular cell can interact only with a membrane point in the same or in a neighboring cell, where all 26 cells that touch a given cell (even at only a corner) are included as neighbors. The actual amount of work required will now depend on the spatial distribution of solute particles and membrane points, but it is clear that in many cases it will be drastically less than $N_\nu N_p$.

3.4. Spatial discretization. The spatial discretization of our system is as follows. At time $t > 0$ and at the Eulerian position $\boldsymbol{x}$, let the fluid velocity be denoted by $\boldsymbol{u}(\boldsymbol{x}, t)$ and the pressure by $p(\boldsymbol{x}, t)$. The fluid variables $\boldsymbol{u}$ and p are represented with periodic boundary conditions in all three directions. Let

$$(3.17) \qquad \boldsymbol{u}_{\mathbf{m}}(t) = \boldsymbol{u}(\mathbf{m}h, t),$$

where h is the grid width, and $\mathbf{m} = (m_1, m_2, m_3)$ is a vector with integer components, and similarly let

$$(3.18) \qquad p_{\mathbf{m}}(t) = p(\mathbf{m}h, t),$$

$$(3.19) \qquad (\boldsymbol{f}_{\text{total}})_{\mathbf{m}}(t) = \boldsymbol{f}_{\text{total}}(\mathbf{m}h, t).$$

Then the spatial discretization of (2.33) and (2.34) is

$$(3.20) \qquad \rho \frac{\partial \boldsymbol{u}_{\mathbf{m}}(t)}{\partial t} + [\mathbf{D}^h p]_{\mathbf{m}}(t) = \mu[\mathbf{L}^h \boldsymbol{u}]_{\mathbf{m}}(t) + (\boldsymbol{f}_{\text{total}})_{\mathbf{m}}(t),$$

$$(3.21) \qquad \mathbf{D}^h \cdot \boldsymbol{u}_{\mathbf{m}}(t) = 0,$$

where we define the discrete gradient, Laplacian, and divergence in the following way:

$$(3.22) \qquad \left[\mathbf{D}^h p\right]_{\mathbf{m}}(t) = \sum_{\alpha=1}^{3} \frac{p_{\mathbf{m}+\mathbf{e}_\alpha}(t) - p_{\mathbf{m}-\mathbf{e}_\alpha}(t)}{2h},$$

$$(3.23) \qquad \left[\mathbf{L}^h \boldsymbol{u}\right]_{\mathbf{m}}(t) = \sum_{\alpha=1}^{3} \frac{\boldsymbol{u}_{\mathbf{m}+\mathbf{e}_\alpha}(t) + \boldsymbol{u}_{\mathbf{m}-\mathbf{e}_\alpha}(t) - 2\boldsymbol{u}_{\mathbf{m}}(t)}{h^2},$$

$$(3.24) \qquad \mathbf{D}^h \cdot \boldsymbol{u}_{\mathbf{m}}(t) = \sum_{\alpha=1}^{3} \frac{\boldsymbol{u}_{\mathbf{m}+\mathbf{e}_\alpha}(t) - \boldsymbol{u}_{\mathbf{m}-\mathbf{e}_\alpha}(t)}{2h} \cdot \mathbf{e}_\alpha.$$

Here $\{\mathbf{e}_\alpha : \alpha = 1, 2, 3\}$ is the standard basis of $\mathbb{R}^3$.

We remark that we could have used a spectral discretization in space. We have instead chosen a spatial discretization that is motivated by considering a finite volume formulation of the fluid-structure equations. This ensures that our discrete numerical methods—even with truncation error—transfer momentum through a local flux while globally conserving the fluid-structure momentum.

Recall that the spreading and interpolation operators Γ_{memb}, Γ_{prt}, and Λ account for the conversion between Lagrangian and Eulerian coordinates. We denote the spreading forces and interpolated velocity by

$$\boldsymbol{f}_{\text{elastic}} := \widetilde{\Lambda} \mathbf{F} \tag{3.25}$$

and

$$\mathbf{U}(\mathbf{X}_{\text{memb}}^{(\ell)}(t), t) := \widetilde{\Gamma}_{\text{memb}} \boldsymbol{u} \quad \text{and} \quad \mathbf{U}(\mathbf{X}_{\text{prt}}^{(k)}(t), t) := \widetilde{\Gamma}_{\text{prt}} \boldsymbol{u}, \tag{3.26}$$

respectively. We use the lattice versions of $\widetilde{\Gamma}_{\text{memb}}$, $\widetilde{\Gamma}_{\text{prt}}$, and $\widetilde{\Lambda}$, and replace the integrals with the corresponding sums. That is, (2.29), (2.30), and (2.31) are discretized as follows:

$$\widetilde{\Lambda} \mathbf{F} = \boldsymbol{f}_{\mathbf{m}, \text{elastic}}(t) = \sum_{k=1}^{N_\nu} \mathbf{F}^{(k)}(t) \, \delta_c\left(\boldsymbol{x}_{\mathbf{m}} - \mathbf{X}^{(k)}(t)\right), \tag{3.27}$$

$$\widetilde{\Gamma}_{\text{memb}} \boldsymbol{u} = \mathbf{U}(\mathbf{X}_{\text{memb}}^{(\ell)}(t), t) = \sum_{\mathbf{m}} \boldsymbol{u}_{\mathbf{m}}(t) \, \delta_c\left(\boldsymbol{x}_{\mathbf{m}} - \mathbf{X}_{\text{memb}}^{(\ell)}(t)\right) h^3, \tag{3.28}$$

$$\widetilde{\Gamma}_{\text{prt}} \boldsymbol{u} = \mathbf{U}(\mathbf{X}_{\text{prt}}^{(k)}(t), t) = \sum_{\mathbf{m}} \boldsymbol{u}_{\mathbf{m}}(t) \, \delta_c\left(\boldsymbol{x}_{\mathbf{m}} - \mathbf{X}_{\text{prt}}^{(k)}(t)\right) h^3, \tag{3.29}$$

where

$$\mathbf{F}^{(k)}(t) = -\frac{\partial \widetilde{\mathcal{E}}[\mathbf{X}(t)]}{\partial \mathbf{X}^{(k)}(t)}, \tag{3.30}$$

or simply

$$\mathbf{F}(t) = -\nabla_{\mathbf{X}} \widetilde{\mathcal{E}}[\mathbf{X}(t)]. \tag{3.31}$$

The term $(\nabla_{\mathbf{X}} \cdot \Lambda) k_{\text{B}} T$ in (2.38) is the local divergence in the configuration $\mathbf{X}$ of the spreading operator Λ. It is evaluated as follows, using c and h interchangeably since later on we will set $c = h$:

$$\begin{aligned}
& k_{\text{B}} T \left(\nabla_{\mathbf{X}} \cdot \widetilde{\Lambda} \right)_{\mathbf{m}} \\
= \; & -\frac{k_{\text{B}} T}{h^4} \sum_{k=1}^{N_\nu} \left[\begin{array}{c}
\varphi'\left(\frac{\boldsymbol{x}_{\mathbf{m}}^{(1)} - \mathbf{X}^{(k,1)}}{h}\right) \varphi\left(\frac{\boldsymbol{x}_{\mathbf{m}}^{(2)} - \mathbf{X}^{(k,2)}}{h}\right) \varphi\left(\frac{\boldsymbol{x}_{\mathbf{m}}^{(3)} - \mathbf{X}^{(k,3)}}{h}\right) \\
\varphi\left(\frac{\boldsymbol{x}_{\mathbf{m}}^{(1)} - \mathbf{X}^{(k,1)}}{h}\right) \varphi'\left(\frac{\boldsymbol{x}_{\mathbf{m}}^{(2)} - \mathbf{X}^{(k,2)}}{h}\right) \varphi\left(\frac{\boldsymbol{x}_{\mathbf{m}}^{(3)} - \mathbf{X}^{(k,3)}}{h}\right) \\
\varphi\left(\frac{\boldsymbol{x}_{\mathbf{m}}^{(1)} - \mathbf{X}^{(k,1)}}{h}\right) \varphi\left(\frac{\boldsymbol{x}_{\mathbf{m}}^{(2)} - \mathbf{X}^{(k,2)}}{h}\right) \varphi'\left(\frac{\boldsymbol{x}_{\mathbf{m}}^{(3)} - \mathbf{X}^{(k,3)}}{h}\right)
\end{array} \right],
\end{aligned} \tag{3.32}$$

where φ and φ' are defined as in (3.7) and (3.8). We denote

$$\boldsymbol{f}_{\mathbf{m}, \text{struc}} := k_{\text{B}} T \left(\nabla_{\mathbf{X}} \cdot \widetilde{\Lambda} \right)_{\mathbf{m}}, \tag{3.33}$$

and combining with $\boldsymbol{f}_{\mathbf{m},\text{elastic}}$, we write

$$(3.34) \qquad \boldsymbol{f}_{\mathbf{m}}\left(t\right) = \boldsymbol{f}_{\mathbf{m},\text{elastic}}\left(t\right) + \boldsymbol{f}_{\mathbf{m},\text{struc}}\left(t\right).$$

Using the finite difference operators (3.27)–(3.29), the whole spatially discretized system becomes

$$(3.35) \qquad \rho\frac{\partial \boldsymbol{u}_{\mathbf{m}}}{\partial t} + [\mathbf{D}^{h}p]_{\mathbf{m}} = \mu[\mathbf{L}^{h}\boldsymbol{u}]_{\mathbf{m}} + \boldsymbol{f}_{\mathbf{m},\text{total}},$$

$$(3.36) \qquad \mathbf{D}^{h}\cdot\boldsymbol{u}_{\mathbf{m}} = 0,$$

$$(3.37) \qquad \widetilde{\mathcal{E}}\left[\mathbf{X}\right] = \widetilde{\mathcal{E}}_{\text{bend}}\left[\mathbf{X}\right] + \widetilde{\mathcal{E}}_{\text{tension}}\left[\mathbf{X}\right] + \widetilde{\mathcal{E}}_{\text{shear}}\left[\mathbf{X}\right] + \widetilde{\Phi}\left(\mathbf{X}\right),$$

$$(3.38) \qquad \mathbf{F}^{(k)} = -\frac{\partial \widetilde{\mathcal{E}}\left[\mathbf{X}\right]}{\partial \mathbf{X}^{(k)}},$$

$$\boldsymbol{f}_{\mathbf{m},\text{total}} = k_{\mathrm{B}}T\left(\nabla_{\mathbf{X}}\cdot\widetilde{\Lambda}\right)_{\mathbf{m}}$$

$$+ \sum_{k=1}^{N_{\nu}}\mathbf{F}^{(k)}\left(t\right)\delta_{c}\left(\boldsymbol{x}_{\mathbf{m}} - \mathbf{X}^{(k)}\left(t\right)\right) + \boldsymbol{g}_{\mathbf{m},\text{thm}}$$

$$(3.39) \qquad = \boldsymbol{f}_{\mathbf{m}} + \boldsymbol{g}_{\mathbf{m},\text{thm}},$$

$$(3.40) \qquad \frac{\partial \mathbf{X}^{(k)}}{\partial t} = \mathbf{U}^{(k)} + \Upsilon^{-1}\left(\mathbf{F}^{(k)} + \mathbf{F}_{\text{thm}}^{(k)}\right).$$

3.5. Temporal discretization. For our numerical simulations, the spatially discretized system of equations must be further discretized in time. Since there is no nonlinear advection in the time-dependent Stokes equations and we use periodic boundary conditions, the fluid solver can be entirely based on the discrete Fourier transform (DFT). The forward and backward DFTs over the N^{3} lattice points are defined by following formulae:

$$(3.41) \qquad \hat{u}_{\mathbf{k}} = \frac{1}{N^{3}}\sum_{\mathbf{m}}\boldsymbol{u}_{\mathbf{m}}e^{-2\pi i\mathbf{m}\cdot\mathbf{k}/N},$$

$$(3.42) \qquad \boldsymbol{u}_{\mathbf{m}} = \sum_{\mathbf{k}}\hat{u}_{\mathbf{k}}e^{2\pi i\mathbf{m}\cdot\mathbf{k}/N},$$

where $0 \leq k_{\alpha} \leq N-1$ and $0 \leq m_{\alpha} \leq N-1$ for $\alpha = 1,2,3$ representing the Cartesian components of the indicated vectors, for instance, $\mathbf{k} = (k_{1}, k_{2}, k_{3}) \in \mathbb{R}^{3}$.

To solve (3.35)–(3.36), we use a projection scheme to satisfy the incompressibility constraint. In the discrete Fourier domain, the discrete equations (3.35)–(3.36) become

$$(3.43) \qquad \frac{\partial \hat{u}_{\mathbf{k}}}{\partial t} + \frac{1}{\rho}\hat{\mathbf{D}}_{\mathbf{k}}\hat{p}_{\mathbf{k}} = -\frac{1}{\tau_{\mathbf{k}}}\hat{u}_{\mathbf{k}} + \frac{1}{\rho}\hat{\boldsymbol{f}}_{\mathbf{k},\text{total}},$$

$$(3.44) \qquad \hat{\mathbf{D}}_{\mathbf{k}}\cdot\hat{u}_{\mathbf{k}} = 0,$$

where the discrete gradient and $-\mu/\rho$ times the Laplacian in the frequency domain are given by

$$(3.45) \qquad \hat{\mathbf{D}}_{\mathbf{k}} = \frac{i}{h}\sin\left(\frac{2\pi\mathbf{k}}{N}\right),$$

$$(3.46) \qquad \tau_{\mathbf{k}} = 1 \left/ \frac{4\mu}{\rho h^{2}}\sum_{\alpha=1}^{3}\left(\sin\left(\frac{\pi k_{\alpha}}{N}\right)\right)^{2}\right..$$

In (3.45), the sine function is applied to a vector by applying it to each component, so that the α component of $\sin(2\pi\mathbf{k}/N)$ is $\sin(2\pi k_\alpha/N)$ for $\alpha = 1, 2, 3$.

We also define two operators, the projection onto the $\hat{\mathbf{D}}_\mathbf{k}$ direction and the projection onto the plane orthogonal to the $\hat{\mathbf{D}}_\mathbf{k}$ direction:

$$(3.47) \qquad \mathcal{P}_\mathbf{k}^{\shortparallel} := \frac{\hat{\mathbf{D}}_\mathbf{k} \cdot \hat{\mathbf{D}}_\mathbf{k}^T}{\left\|\hat{\mathbf{D}}_\mathbf{k}\right\|^2} \quad \text{and} \quad \mathcal{P}_\mathbf{k}^{\perp} := \mathcal{I} - \frac{\hat{\mathbf{D}}_\mathbf{k} \cdot \hat{\mathbf{D}}_\mathbf{k}^T}{\left\|\hat{\mathbf{D}}_\mathbf{k}\right\|^2}.$$

To ensure that the above notation is well defined, for the set of modes $\mathcal{K}$ for which $\hat{\mathbf{D}}_\mathbf{k} = \mathbf{0}$, we set the corresponding operators $\mathcal{P}_\mathbf{k}^{\shortparallel} = \mathbf{0}$ and $\mathcal{P}_\mathbf{k}^{\perp} = \mathcal{I}$. This set is given by

$$(3.48) \qquad \mathcal{K} = \{\mathbf{k} = (k_1, k_2, k_3) \mid k_\alpha = 0 \text{ or } N/2 \text{ for } \alpha = 1, 2, 3\}.$$

Note that, for all $\mathbf{k}$, $\hat{\mathbf{D}}_\mathbf{k} \cdot \hat{\boldsymbol{u}}_\mathbf{k} = 0$ by incompressibility, and therefore $\hat{\mathbf{D}}_\mathbf{k} \cdot \partial_t \hat{\boldsymbol{u}}_\mathbf{k} = 0$. For any $t > 0$, the pressure can be derived by taking an inner product with $\hat{\mathbf{D}}_\mathbf{k}$ on both sides of (3.43):

$$(3.49) \qquad \hat{p}_\mathbf{k} = \begin{cases} \frac{-\hat{\mathbf{D}}_\mathbf{k} \cdot \hat{\boldsymbol{f}}_{\mathbf{k},\text{total}}}{\left\|\hat{\mathbf{D}}_\mathbf{k}\right\|^2}, & \mathbf{k} \neq \mathcal{K}, \\ 0, & \mathbf{k} \in \mathcal{K}. \end{cases}$$

In the sense of the Itô calculus notation, the fluid equations with both structure and thermal forces can be expressed as shown in [17, 24], in the following way:

$$\begin{aligned}(3.50) \qquad d\hat{\boldsymbol{u}}_\mathbf{k} &= -\frac{1}{\tau_\mathbf{k}}\hat{\boldsymbol{u}}_\mathbf{k}dt + \rho^{-1}\mathcal{P}_\mathbf{k}^{\perp}\hat{\boldsymbol{f}}_{\mathbf{k},\text{total}}dt \\ &= \left(-\frac{1}{\tau_\mathbf{k}}\hat{\boldsymbol{u}}_\mathbf{k} + \frac{1}{\rho}\mathcal{P}_\mathbf{k}^{\perp}\hat{\boldsymbol{f}}_\mathbf{k}\right)dt + \sqrt{2\xi_\mathbf{k}}\mathcal{P}_\mathbf{k}^{\perp}d\widetilde{\mathbf{B}}_\mathbf{k}(t),\end{aligned}$$

where $d\widetilde{\mathbf{B}}_\mathbf{k}$ represents a three-dimensional complex-valued Brownian motion, with the constraint $\overline{d\widetilde{\mathbf{B}}_{\mathbf{N}-\mathbf{k}}} = d\widetilde{\mathbf{B}}_\mathbf{k}$ to ensure that the thermal forcing is real-valued, where $\mathbf{N} = (N, N, N)$. Based on the covariance structure (2.25)–(2.27), the thermal forcing coefficient is given by

$$(3.51) \qquad \xi_\mathbf{k} = \begin{cases} \frac{k_\mathrm{B}T}{\rho L^3 \tau_\mathbf{k}} & \text{for } \mathbf{k} \in \mathcal{K}, \\ \frac{k_\mathrm{B}T}{2\rho L^3 \tau_\mathbf{k}} & \text{for } \mathbf{k} \notin \mathcal{K}. \end{cases}$$

In the temporal discretization, we use the same increment Δt for all time steps, and the state variables at the nth time step corresponding to the time $t_n = n\Delta t$ are denoted by a superscript integer n. We take the instantaneous force to be constant over the time increment Δt. The procedure by which the fluid velocity is updated from one time step to the next is described analytically by the following recurrence relation based on an exponential time stepping scheme [24]:

$$(3.52) \qquad \hat{\boldsymbol{u}}_\mathbf{k}^{n+1} = a_\mathbf{k}\hat{\boldsymbol{u}}_\mathbf{k}^n + \frac{(1 - a_\mathbf{k})}{\rho}\tau_\mathbf{k}\mathcal{P}_\mathbf{k}^{\perp}\hat{\boldsymbol{f}}_\mathbf{k}^n + \mathcal{P}_\mathbf{k}^{\perp}\hat{\boldsymbol{\Xi}}_\mathbf{k}^n,$$

where

$$(3.53) \qquad a_\mathbf{k} := e^{-\Delta t/\tau_\mathbf{k}} \quad \text{and where} \quad \hat{\boldsymbol{\Xi}}_\mathbf{k}^n = \sigma_\mathbf{k}\hat{\mathbf{G}}_\mathbf{k},$$

accounts for the thermal fluctuations over the time step. Here, the random variable $\hat{\boldsymbol{G}}_{\mathbf{k}}$ is obtained by generating a three-dimensional complex-valued standard Gaussian random variable with mean 0, variance 1, and independent real and imaginary components for each Fourier mode $\mathbf{k}$. The variance of $\hat{\boldsymbol{\Xi}}_{\mathbf{k}}^{n}$ is therefore given by

$$(3.54) \qquad\qquad \sigma_{\mathbf{k}}^{2} = \xi_{\mathbf{k}} \tau_{\mathbf{k}} \left(1 - a_{\mathbf{k}}^{2}\right).$$

Upon discretizing (3.40) in time, the immersed boundary positions $\mathbf{X}^{n,(k)}$ are updated by

$$\mathbf{X}^{n+1,(k)} = \mathbf{X}^{n,(k)} + \sum_{\mathbf{m}} \delta_{c} \left(\boldsymbol{x}_{\mathbf{m}} - \mathbf{X}^{n,(k)}\right) h^{3} \int_{t_{n}}^{t_{n+1}} \boldsymbol{u}_{\mathbf{m}}\left(s\right) ds$$

$$(3.55) \qquad\qquad + \Delta t \Upsilon^{-1} \left(\mathbf{F}^{n,(k)} + \mathbf{F}_{\text{thm}}^{n,(k)}\right),$$

where

$$(3.56) \qquad\qquad t_{n} = n\Delta t \quad\text{and}\quad \mathbf{X}^{n,(k)} = \mathbf{X}^{(k)}\left(n\Delta t\right),$$

and similarly for all Lagrangian variables. In (3.55), the fluid velocity $\boldsymbol{u}_{\mathbf{m}}(s)$ is integrated to resolve the dynamics of the Fourier modes of the fluid. We define

$$(3.57) \qquad\qquad \boldsymbol{\Omega}_{\mathbf{m}}^{n} = \int_{t_{n}}^{t_{n+1}} \boldsymbol{u}_{\mathbf{m}}\left(s\right) ds.$$

To update the position of the structure, as discussed in section 3.3.5 of [24], $\hat{\boldsymbol{\Omega}}_{\mathbf{k}}^{n}$ can be expressed in the Fourier domain as

$$(3.58) \qquad\qquad \hat{\boldsymbol{\Omega}}_{\mathbf{k}}^{n} = \hat{\mathbf{H}}_{\mathbf{k}} + c_{1,\mathbf{k}} \mathcal{P}_{\mathbf{k}}^{\perp} \hat{\boldsymbol{\Xi}}_{\mathbf{k}}^{n} + c_{2,\mathbf{k}} \mathcal{P}_{\mathbf{k}}^{\perp} \hat{\mathbf{G}}_{\mathbf{k}},$$

where $\hat{\boldsymbol{\Xi}}_{\mathbf{k}}^{n}$ has been defined above, and

$$(3.59) \qquad\qquad \hat{\mathbf{H}}_{\mathbf{k}} = \tau_{\mathbf{k}} \left[\left(1 - a_{\mathbf{k}}\right) \hat{\boldsymbol{u}}_{\mathbf{k}}^{n} + \left(\Delta t - \tau_{\mathbf{k}}\left(1 - a_{\mathbf{k}}\right)\right) \rho^{-1} \mathcal{P}_{\mathbf{k}}^{\perp} \hat{\boldsymbol{f}}_{\mathbf{k}}^{n}\right].$$

The two sets of coefficients in (3.58) are given by

$$(3.60) \qquad c_{1,\mathbf{k}} = \tau_{\mathbf{k}} \tanh\left(\frac{\Delta t}{2\tau_{\mathbf{k}}}\right) \quad\text{and}\quad c_{2,\mathbf{k}} = \sqrt{2\xi_{\mathbf{k}} \tau_{\mathbf{k}}^{2} \left(\Delta t - 2c_{1,\mathbf{k}}\right)}.$$

In this manner, (3.55) becomes

$$(3.61) \qquad \mathbf{X}^{n+1,(k)} = \mathbf{X}^{n,(k)} + \widetilde{\Gamma}\left[\boldsymbol{\Omega}_{\mathbf{k}}^{n}\right] + \Delta t \Upsilon^{-1}\left(\mathbf{F}^{n,(k)} + \sqrt{\frac{2\Upsilon k_{\mathrm{B}}T}{\Delta t}} \mathcal{N}\right),$$

where we have approximated $\mathbf{F}_{\text{thm}}^{n,(k)}$ by

$$(3.62) \qquad\qquad \mathbf{F}_{\text{thm}}^{n,(k)} = \sqrt{\frac{2\Upsilon k_{\mathrm{B}}T}{\Delta t}} \mathcal{N},$$

and $\mathcal{N}$ is a three-dimensional real-valued Gaussian random variable with independent components, each of which has mean 0 and variance 1. Notice that when the time

step is taken small, the temporal integrator presented in (3.61) has weak first order accuracy. A detailed error analysis is given in [33].

We remark here that the reason we represent our fluid velocity field in a Fourier series is twofold. First, we use the fast Fourier transform and symbols of the discrete Laplacian (as discretized by the finite volume method) to solve efficiently the pressure equations that impose incompressibility of the fluid. Second, we use the Fourier series representation of the time-dependent velocity field to develop an efficient stochastic integrator for the temporal dynamics of the PDE. The linear fluid equations decompose in Fourier space into a system of first order ODEs that can be partially integrated analytically using exponential factors. This is the basis of our numerical methods that overcome stiffness in the temporal dynamics, allowing us to use comparatively large time steps relative to the relaxation time-scales of the fast fluid modes.

4. Numerical experiments in equilibrium statistical mechanics. In order to validate our methodology and assess its accuracy, in this section we give several numerical examples of processes in thermodynamic equilibrium.

4.1. Temperature. The stochastic forces were introduced to model the system as if it were in contact with a heat reservoir at a prescribed temperature. We check in practice our stochastic thermostatting. This can be done by considering the amount of kinetic energy per fluid degree of freedom. According to the equipartition theorem of classical statistical mechanics, each degree of freedom contributes a kinetic energy of $\frac{1}{2}k_{\mathrm{B}}T$ at thermal equilibrium. The kinetic energy per unit volume is given by

$$(4.1) \qquad \frac{\rho}{2}\left\|\boldsymbol{u}\right\|^2 = \frac{\rho}{2}\left(u_1^2 + u_2^2 + u_3^2\right),$$

and the total kinetic energy can be calculated by integrating over the entire fluid domain. Of course, we can discretize this integral by defining a grid with cell volume h^3 on which the integral becomes

$$(4.2) \qquad \frac{\rho}{2}\sum_{\mathbf{m}}\left\|\boldsymbol{u}_{\mathbf{m}}\right\|^2 h^3.$$

If the grid is $N \times N \times N$, the number of degrees of freedom is

$$(4.3) \qquad 2(N^3 - 8) + 3 \times 8 = 2(N^3 + 4).$$

Note that, in the calculation of the number of degrees of freedom, the factor that multiplies N^3 is 2, not 3, even though there are three components of velocity. This is because the velocity has to be divergence-free, and this removes one degree of freedom per grid point. In the above formula, there are eight modes that are multiplied by 3 instead of 2. This is because these modes are automatically divergence-free.
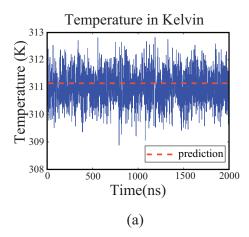
Thus, the kinetic energy of the fluid is expected to be

$$(4.4) \qquad 2(N^3 + 4)\frac{1}{2}k_{\mathrm{B}}T = (N^3 + 4)k_{\mathrm{B}}T.$$

Putting all of the above together, one gets an output temperature (like putting a thermometer in the fluid) at each time step, which may be averaged over many time steps and compared to the input temperature. This is a good check of whether the method controls the system temperature correctly.

Setting the kinetic energy (4.2) and (4.4) to be equal and solving for T, we have

$$(4.5) \qquad T(t) = \frac{\frac{\rho}{2}\sum_{\mathbf{m}}\left\|\boldsymbol{u}_{\mathbf{m}}(t)\right\|^2 h^3}{(N^3 + 4)k_{\mathrm{B}}}.$$
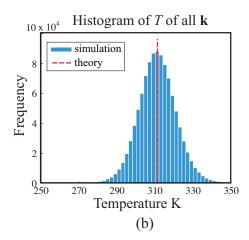
FIG. 2. (a) *The temperature in the simulation of the system fluctuates around the input temperature setting of 311.16 K. The test is done with a vesicle and solute particles in the simulation.* (b) *Histogram of the temperatures of all the Fourier modes. The simulation was run with the parameters $N = 256$, $L = 2000$ nm, $T = 311.16$ K, $\Delta t = 1$ ns. 2,000 time steps were simulated.*

As shown in Figure 2, the actual temperature in our simulation fluctuates around the input temperature setting. In fact the average temperature over 2000 ns is 311.1587, which differs by merely 0.000421% from the input temperature setting.

Statistical mechanics and thermodynamics interpret temperature as an observable quantity associated with the ensemble instead of any particular microstate of the system. While it is true that for a collection of particles the average kinetic energy does appear to manifest properties similar to those of the temperature, the actual instantaneous kinetic energy fluctuates significantly. It is not until we consider a system that is either infinitely large or an average over time that we get a meaningful value for the temperature.

As discussed in [21, 24], the temperature is imposed on the ensemble of particles/structures. Here we explicitly thermostat the system by our choice of stochastic driving fields to achieve a given target temperature. This is done in the sense that we obtain a particular Boltzmann ensemble for the probability distribution of microstates of the system. That is the sense in which temperature T has meaning, not instantaneous microstates or instantaneous kinetic energy. With that said, there are further estimators that can be constructed to compute T from simulation trajectories to verify the implementation of the thermostat.

Now, we validate the equilibrium "temperature" (variance) of each of the Fourier modes, not just the total kinetic energy. We assign to each mode a "temperature" based on each empirical variance, i.e.,

$$(4.6) \qquad \left\langle |\hat{\boldsymbol{u}}_{\mathbf{k}}|^2 \right\rangle = \begin{cases} \frac{3k_{\mathrm{B}}T_{\mathbf{k}}}{\rho L^3}, & \mathbf{k} \in \mathcal{K}, \\ \frac{2k_{\mathrm{B}}T_{\mathbf{k}}}{\rho L^3}, & \mathbf{k} \notin \mathcal{K}, \end{cases}$$

or rearrange terms, i.e.,

$$(4.7) \qquad T_{\mathbf{k}} = \begin{cases} \frac{\rho L^3 \left\langle |\hat{\boldsymbol{u}}_{\mathbf{k}}|^2 \right\rangle}{3k_{\mathrm{B}}}, & \mathbf{k} \in \mathcal{K}, \\ \frac{\rho L^3 \left\langle |\hat{\boldsymbol{u}}_{\mathbf{k}}|^2 \right\rangle}{2k_{\mathrm{B}}}, & \mathbf{k} \notin \mathcal{K}. \end{cases}$$

Notice that (4.7) is not an actual thermodynamic temperature but simply an approximation for the magnitude of the energy fluctuations—temperature here is constant by definition, and energy fluctuates. In theory, if a very small time step were adopted, and statistical errors were eliminated in the sense of an average over a significantly long time, the distribution of temperatures would be a delta function. A histogram of all the Fourier modes is shown in Figure 2(b).

4.2. Spherically symmetric potential. As a preliminary test before considering the full vesicle, we consider particles confined in a spherically symmetric potential given by

$$(4.8) \qquad \mathcal{E}_R \left[\|\mathbf{X}_{\mathrm{prt}}\| \right] = \lambda \sum_{k=1}^{N_p} \varphi_c \left(\left\| \mathbf{X}_{\mathrm{prt}}^{(k)} \right\| - R \right),$$

where $\mathbf{X}_{\mathrm{prt}}^{(k)}$ is the position of the kth solute particle, N_p is the number of particles, R is the radius of an imaginary vesicle, and φ_R is the kernel function as defined in (3.7). Note that in this setup there is actually no vesicle, but rather a potential barrier. To avoid leakage of the solute particles, λ is chosen so that as a single particle passes through the vesicle from position $R - c$ to position R, the energy changes by roughly $15 k_{\mathrm{B}} T$.

The forces exerted on the wall can be easily computed by taking the gradient of (4.8), and thus the osmotic wall pressure is defined as the time average of the sum of the normal forces exerted by the solute particles divided by the area of the wall [27],

$$(4.9) \qquad \langle p_{\mathrm{wall}} \rangle = \frac{1}{4 \pi R^2} \left\langle \sum_{k=1}^{N_p} -\mathbf{F}^{(k)} \cdot \hat{\mathbf{n}}^{(k)} \right\rangle,$$

where

$$(4.10) \qquad \hat{\mathbf{n}}^{(k)} = \mathbf{X}_{\mathrm{prt}}^{(k)} / \left\| \mathbf{X}_{\mathrm{prt}}^{(k)} \right\|,$$
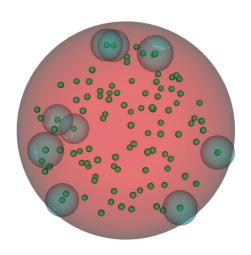
since the spherically symmetric potential is centered about the origin.

We simulated 100 solute particles confined by the spherically symmetric potential, and the osmotic wall pressure in the equilibrium state should obey Van 't Hoff's law,

$$(4.11) \qquad \langle p_{\mathrm{wall}} \rangle = \frac{N_p}{V} k_{\mathrm{B}} T \approx 31.6225 \left(\mathrm{amu \cdot n} m^{-1} \mathrm{n} s^{-2} \right).$$

We ran our simulations for 10000 ns and found good agreement with Van 't Hoff's law, as shown in Figure 3.

4.3. Equilibrium size. In this section, we present a variety of simulations of a semipermeable elastic vesicle immersed in an incompressible viscous fluid. Given the initial temperature of the system, we determine the corresponding kinetic energy of the system, as well as the initial mean deformation velocity of the elastic shell and mean elastic forces. Statistically speaking, the vesicle's equilibrium size should be determined by a balance between the osmotic pressure and surface tension. (Recall that the bending energy and shear energy are scale-invariant for a sphere, and so they are not expected to contribute to the osmotic force balance.) If the initial size of the vesicle is too large, it should shrink; if it is too small, it should grow. Actually, we can
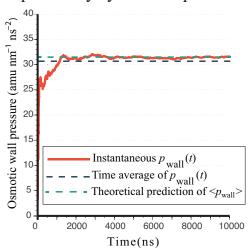
Spherically symmetric potential

FIG. 3. *The solute particles are confined by a spherically symmetric potential. As the fluctuating solute particles get within a distance c of the wall, as illustrated by the shaded spheres around the solute particles, they begin interacting with the potential. The solute particles are pushed back inward, and thus confined to the vesicle. The dashed line of the time average of $p_{\mathrm{wall}}(t)$ is slightly lower than the theoretical prediction of $\langle p_{\mathrm{wall}}\rangle$ since the solute particles create no wall pressure at the initial state until reaching an equilibrium at time 1750 (ns).*

estimate the equilibrium size. From Van 't Hoff's law, the osmotic pressure depends on the volume V (or, equivalently, the concentration C) according to

$$(4.12) \qquad p_{\mathrm{osmotic}} = k_{\mathrm{B}}TC = k_{\mathrm{B}}T\frac{N_p}{V}.$$

On the other hand, given the radius of the vesicle, the pressure can be found analytically from the elasticity law. The work done by the elastic pressure, $p_{\mathrm{elastic}}dV$, is the work done on the elastic membrane, which is converted into elastic energy. Thus $p_{\mathrm{elastic}}dV$ must equal the infinitesimal change in the elastic energy, so that

$$(4.13) \qquad p_{\mathrm{elastic}}dV = \mathcal{E}'(V)\,dV,$$

or

$$(4.14) \qquad k_{\mathrm{B}}TN_p = V\mathcal{E}'(V).$$

Here, $\mathcal{E}(V)$ denotes the elastic energy of the vesicle as a function of its volume V, and $\mathcal{E}'(V)$ is the derivative of $\mathcal{E}$ with respect to V. Since $\mathcal{E}'(V) > 0$, (4.14) has a unique solution V for every choice of N_p.

We approximate $\mathcal{E}(V)$ by assuming that the vesicle is spherical. In that case, as remarked above, the bending and shear energies are scale-invariant, i.e., independent of V, so the only contribution to $\mathcal{E}(V)$ comes from the surface-tension energy, which is $\sigma 4\pi R^2$, where R is the radius of a sphere of volume V, so that

$$(4.15) \qquad R = \left(\frac{V}{\frac{4}{3}\pi}\right)^{1/3}.$$

TABLE 1
Numerical results for different numbers of solute particles N_p.

N_p	$R_{\text{simulation}}$ (nm)	R_{theory} (nm)	$p_{\text{simulation}}\left(\frac{\text{amu}}{\text{ns}^2\text{nm}}\right)$	$p_{\text{theory}}\left(\frac{\text{amu}}{\text{ns}^2\text{nm}}\right)$
50	70.7333	70.7107	93.8278	87.2598
100	99.1332	100.0000	68.8845	63.3955
200	137.8191	141.4214	44.4221	47.1865
300	169.8998	173.2051	33.2902	37.7785

Thus

$$\mathcal{E}(V) = \sigma 4\pi \left(\frac{V}{\frac{4}{3}\pi}\right)^{2/3}, \tag{4.16}$$

and

$$\mathcal{E}'(V) = \frac{8\pi\sigma}{3}\left(\frac{V}{\frac{4}{3}\pi}\right)^{-1/3}\frac{1}{\frac{4}{3}\pi} = 2\sigma\left(\frac{V}{\frac{4}{3}\pi}\right)^{-1/3} = \frac{2\sigma}{R}. \tag{4.17}$$

Substituting this result into (4.14) gives

$$k_{\text{B}}TN_p = \frac{4}{3}\pi R^3 \frac{2\sigma}{R} = \frac{8\pi R^2\sigma}{3}, \tag{4.18}$$

which shows that the effective radius[1] of the vesicle at equilibrium is given by

$$R = \sqrt{\frac{3k_{\text{B}}TN_p}{8\pi\sigma}}. \tag{4.19}$$

Also, the osmotic pressure at equilibrium is given by

$$p = \frac{k_{\text{B}}TN_p}{V} = \left(\frac{3}{4\pi}\right)\left(\frac{8\pi\sigma}{3}\right)^{3/2}(k_{\text{B}}TN_p)^{-1/2}. \tag{4.20}$$

It is a striking prediction that the osmotic pressure *decreases* with increasing N_p. This is because the vesicle is increasing in volume, and the resulting reduction in curvature makes the surface tension less effective at generating internal pressure.[2]

Results are shown in Table 1 and Figure 4. The dynamic processes of the swelling/shrinking vesicles due to different numbers of solute particles are shown in Figures 5 and 6. The numerical parameters used in the simulation are shown in Table 2. These parameters are chosen based on realistic values. For instance, the temperature is body temperature in Kelvin, and the bending/shear moduli used are close to their values for biological materials such as DOPC/DPPC [34, 35, 36]. The computed radius of the vesicle is obtained by evaluating the volume contained within the triangulated surface, averaged over time in the steady state, and then finding the radius of a sphere with the same volume. The computed pressures are found by

---

[1]The effective radius of the vesicle is the radius of a sphere that attains the same volume.
[2]Note that this result is peculiar to the particular form of the elastic energy that we have chosen. If the elastic energy increases sufficiently rapidly with increasing vesicle volume, then the osmotic pressure will increase with increasing N_p.
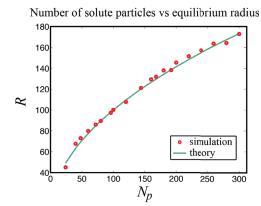
FIG. 4. *For different numbers of solute particles, N_p, the figure shows that the computed equilibrium radii (open symbols) almost coincide with the theoretical prediction (solid line).*

considering the centroid and the exterior of the vesicle:

$$(4.21) \qquad \mathbf{X}_{\text{in}} = \frac{1}{N_\nu} \sum_{\ell=1}^{N_\nu} \mathbf{X}_{\text{memb}}^{(\ell)},$$

$$(4.22) \qquad \mathbf{X}_{\text{out}} = \mathbf{X}_{\text{in}} + \frac{L}{2}\left(\mathbf{e}_1 + \mathbf{e}_2 + \mathbf{e}_3\right),$$

where L is the length of the domain, and $\mathbf{e}_\alpha$ are the unit vectors of a three-dimensional Cartesian coordinate system. Then, the pressure jump is given by the difference of the interpolated pressures at $\mathbf{X}_{\text{in}}$ and $\mathbf{X}_{\text{out}}$:

$$(4.23) \qquad [p(t)] = \sum_{\mathbf{m}} p_{\mathbf{m}} \delta_c(\mathbf{x}_{\mathbf{m}} - \mathbf{X}_{\text{in}})h^3 - \sum_{\mathbf{m}} p_{\mathbf{m}} \delta_c(\mathbf{x}_{\mathbf{m}} - \mathbf{X}_{\text{out}})h^3.$$

4.4. Dimer test. In this section, we take the solute particles contained by the elastic vesicle to be connected pairwise by elastic springs with zero rest length. Then, at some specified time, we transform them by cutting all the springs and observe the resulting change in the size of the vesicle. If the springs are sufficiently stiff (see below), there are effectively twice as many particles after cutting the springs, and the size of the vesicle therefore increases.

As shown in Figure 7, there are initially N dimers, and the immersed vesicle starts swelling when the springs are cut. The vesicle eventually reaches an equilibrium state determined by the surface tension and the osmotic pressure of $2N$ monomers. In Figure 7, there are clearly two equilibrium states: one for the dimers and one for the monomers, even though the total number of solute particles does not change at all. The only difference is the existence of the particle-particle interaction in the dimer state before the springs are cut. We remark that the mechanism illustrated here, in which a chemical reaction is used to change the effective number of solute particles and thereby regulate the volume of a vesicle, could in fact be used within biological cells to regulate the size of vesicles or organelles.

The simulation described above raises an important question. If a pair of particles connected by a spring counts as one particle, and the same pair of particles when not connected by a spring counts as two particles, what happens if we go continuously from one situation to the other by continuously varying the stiffness constant of the

(a) Shrinking vesicle with 50 solute particles

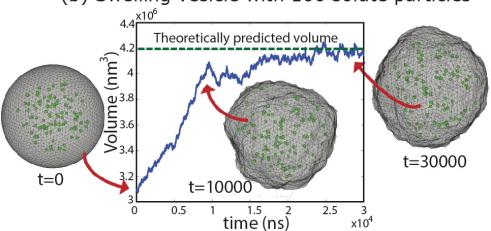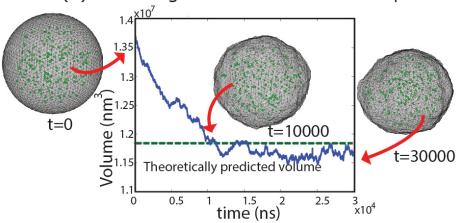

(b) Swelling vesicle with 100 solute particles

FIG. 5. *Initially, N_p solute particles are randomly placed inside the vesicle. The vesicle size approaches the equilibrium size and then fluctuates around equilibrium. The simulations are run up to 30000 ns using different numbers of solute particles:* (a) $N_p = 50$, (b) $N_p = 100$. *Beginning with a larger volume in* (a) *and a smaller volume in* (b), *eventually the vesicle sizes approach their theoretically predicted equilibrium values. The initial volumes of the vesicles are different in the two cases (note different scales on the vertical axes).*

spring? Intuitively, we expect that the equilibrium size of the vesicle should depend continuously on the stiffness constant of the spring. We remark that this contrasts with the Van 't Hoff theory, where only the number of molecules matters, and not the properties of their internal degrees of freedom.

Using statistical mechanics theory, we can express the transition between equilibrium volumes as a function of the spring stiffness. Since we are considering an isothermal system, we begin by writing the Helmholtz free energy in terms of the canonical partition function. This provides the osmotic pressure as a function of the

(a) Shrinking vesicle with 200 solute particles

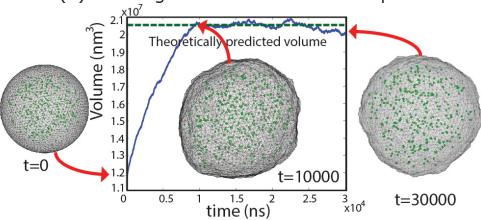## (b) Swelling vesicle with 300 solute particles

FIG. 6. *Vesicles are swelling and shrinking for* (a) $N_p = 200$ *and* (b) $N_p = 300$ *solute molecules with initial volume* 1.39×10^7 *(swelling) and initial volume* 1.17×10^7 *(shrinking), respectively. For the other parameters, the simulations used the same values as the results in Figure* 5.

spring stiffness by taking a partial derivative of the Helmholtz free energy with respect to the equilibrium volume at constant temperature. It is important to note that the thermal fluctuations of the membrane are not taken into account in this theory (only the effective free energy of the contained volume). We assume in the theory that the membrane maintains its spherical shape, although we do allow the sphere to change volume. To obtain our condition of equilibrium, we balance the changes in elastic energy of the membrane, assuming an effectively spherical shape, with the free energy of the confined volume. Despite this approximation in our theory, we get good agreement between the theoretical and computational simulation results.

The computational results are shown in Figure 8, where they are compared to a theoretical curve that is the result of a statistical-mechanical calculation; see Appendix B in the supplementary material. In agreement with physical intuition, but

TABLE 2
Numerical parameters.

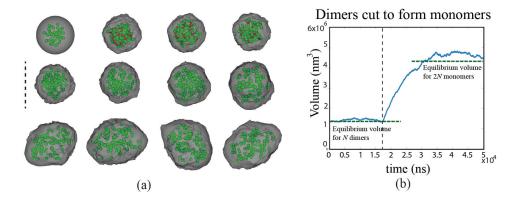| Parameters	Description	Value
T	temperature	311.16 K
L	domain length in each direction	500 nm
k_{B}	Boltzmann's constant	$8314.46 \ \mathrm{nm}^2 \cdot \mathrm{amu} \cdot \mathrm{ns}^{-2}\mathrm{K}^{-1}$
ρ	uniform density of water	$597.98 \ \mathrm{amu} \cdot \mathrm{nm}^{-3}$
μ	dynamic viscosity of water	$4.63 \times 10^5 \ \mathrm{amu} \cdot \mathrm{ns}^{-1} \cdot \mathrm{nm}^{-1}$
σ	surface tension of the membrane	$3088.2 \ \mathrm{amu} \cdot \mathrm{ns}^{-2}$
κ_b	bending modulus	$51525 \ \mathrm{nm}^2 \cdot \mathrm{amu} \cdot \mathrm{ns}^{-2}$
κ_s	shear modulus of the membrane	$2.5871 \times 10^8 \ \mathrm{amu} \cdot \mathrm{ns}^{-2}$
N	number of Eulerian meshwidths in each direction	64
Δt	time step	1 ns
h	nesh width	7.81 nm

(a) (b)

FIG. 7. (a) *Swelling of a vesicle when solute dimers dissociate into monomers. Initially the vesicle contains* 50 *dimers. Each dimer is modeled as a pair of particles connected by a spring. The spring has zero rest length, and initially the two particles coincide, but they move apart because of thermal fluctuations. At* $t = 15\mu s$, *the springs are removed, and the* 50 *dimers become* 100 *monomers. The vesicle swells accordingly. The figure shows the vesicle and solute particles at equally spaced times starting with* $t = 0$ *(upper left) and continuing in increments of* $4.17\mu s$ *from left to right across each row. The event on which the springs are removed (vertical dashed line) occurs between the frame at the end of the first row and the frame at the beginning of the second row.* (b) *Plot of vesicle volume as a function of time for the computer experiment shown in* (a). *Horizontal dashed lines show the theoretical equilibrium volumes for* N *solute particles and for* $2N$ *solute particles. Vertical dashed line indicates time at which dimers were cut to form monomers.*

in disagreement with Van 't Hoff's law, we do indeed see a smooth transition from dimer-like behavior to monomer-like behavior as the stiffness constant is reduced. The transition happens at spring constants which are such that the typical distance at the ambient temperature T between the particles that compose a dimer is comparable to the size of the vesicle that contains them.

The need to account for effects beyond Van 't Hoff's law is fundamental for many microscopic phenomena. In a macroscopic situation there is, by definition of "macroscopic," a huge (in principle, infinite) gap between the size of a solute molecule and the size of the container. Thus, if a spring is present at all, its stiffness cannot be so small that the size of the dimer is comparable to the size of the container. If it were, the container could not be considered macroscopic, since it would have molecular-scale dimension. In some sense, Van 't Hoff's law is valid only macroscopically, and our method can capture these important deviations in the microscopic regime.
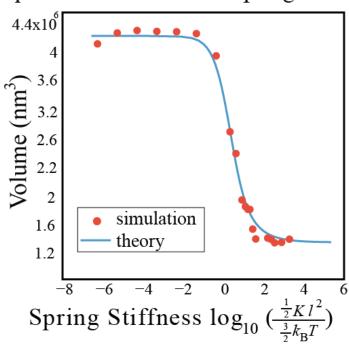
FIG. 8. *Plot of equilibrium vesicle volume for $\frac{1}{2}N_p$ immersed dimers as a function of $\log_{10}\left(\frac{1}{2}K\ell^2/\frac{3}{2}k_BT\right)$, where K is the stiffness of the spring in each dimer, and ℓ is such that $\frac{4}{3}\pi\left(\ell/2\right)^3 = \left(V_{N_{p/2}} + V_{N_p}\right)/2$, where $V_{N_{p/2}}$ and V_{N_p} are the theoretical equilibrium volumes with $N_{p/2}$ solute particles and N_p solute particles, respectively. Note that 0 on the horizontal axis corresponds to the stiffness at which the typical size of each dimer at temperature T is about the same as the vesicle diameter. Symbols are computational results, and the solid line is from a statistical-mechanical theory derived in Appendix B of the supplementary material.*

5. Summary and conclusions. We have introduced computational methods for the direct numerical simulation of osmotic phenomena involving semipermeable elastic structures, hydrodynamic transport, and solute interactions at the particle level. We have used these approaches to investigate the swelling of vesicles having spherical topology and membrane elasticity described by a surface tension, a neo-Hookean shear modulus, and a Helfrich bending modulus. We have shown that our computational model is capable of capturing important osmotic phenomena beyond the classical Van 't Hoff theory. We expect our methods to be useful for the simulation of osmotically driven flows and deformation in a wide class of applications arising in technological systems and biology.

REFERENCES

[1] C. S. PESKIN, *The immersed boundary method*, Acta Numer., 11 (2002), pp. 479–517.
[2] M. NAPOLI, J. C. T. NAPOLI, AND S. PENNATHUR, *Nanofluidic technology for biomolecule applications: A critical review*, Lab Chip, 10 (2010), pp. 957–985.

[3]   D. Voet, J. G. Voet, and C. W. Pratt, *Fundamentals of Biochemistry: Life at the Molecular Level*, Wiley, New York, 2012.

[4]   J. Nardi, R. Bruinsma, and E. Sackmann, *Vesicles as osmotic motors*, Phys. Rev. Lett., 82 (1999), pp. 5168–5171.

[5]   B. J. Sandmann, *Physical properties of solutions*, in Applied Physical Pharmacy, M. M. Amiji and B. J. Sandmann, eds., McGraw-Hill Medical Publishing Division, New York, 2002, pp. 47–66.

[6]   D. D. Loo, E. M. Wright, and T. Zeuthen, *Water pumps*, J. Physiol., 542 (2002), pp. 53–60.

[7]   A. J. Staverman, *The theory of measurement of osmotic pressure*, Recl. Trav. Chim. Pays-Bas, 70 (1951), pp. 344–352.

[8]   J. H. van 't Hoff, *Osmotic pressure and chemical equilibrium* (Nobel lecture, 1901), in Nobel Lectures, Chemistry 1901–1921, Elsevier, Amsterdam, 1966.

[9]   J. H. van 't Hoff, *The role of osmotic pressure in the analogy between solutions and gases*, Z. Phys. Chem., 1 (1887), pp. 481–508.

[10] D. Chandler, *Introduction to Modern Statistical Mechanics*, Oxford University Press, New York, 1987.

[11] A. Einstein, *Investigations on the Theory of the Brownian Movement*, Dover, New York, 1956.

[12] A. Bensoussan and R. Temam, *Équations stochastiques du type Navier-Stokes*, J. Funct. Anal., 13 (1973), pp. 195–222.

[13] Z. Brzeźniak and S. Peszat, *Strong local and global solutions to stochastic Navier-Stokes equations*, in Infinite Dimensional Stochastic Analysis, Proceedings of the Colloquium of the Royal Netherlands Academy of Sciences, Amsterdam, 1999, North–Holland, Amsterdam, 2000, pp. 85–98.

[14] M. Capinski and N. J. Cutland, *Stochastic Navier-Stokes equations*, Acta Appl. Math., 25 (1991), pp. 59–85.

[15] F. Flandoli and D. Gatarek, *Martingale and stationary solutions for stochastic Navier-Stokes equations*, Probab. Theory Related Fields, 102 (1995), pp. 367–391.

[16] A. Inoue and T. Funaki, *On a new derivation of the Navier-Stokes equation*, Comm. Math. Phys., 65 (1979), pp. 83–90.

[17] B. Øksendal, *Stochastic Differential Equations. An Introduction with Applications*, 6th ed., Springer-Verlag, Berlin, 2003.

[18] E. M. Purcell, *Life at low Reynolds number*, Amer. J. Phys., 45 (1977), pp. 3–11.

[19] M. Jardak, C. H. Su, and G. E. Karniadakis, *Spectral polynomial solutions of the stochastic advection equation*, J. Sci. Comput., 17 (2002), pp. 319–338.

[20] M. I. Vishik and A. V. Fursikov, *Mathematical Problems of Statistical Hydromechanics*, Kluwer Academic Publishers, Dordrecht, Boston, London, 1988.

[21] P. J. Atzberger, *Stochastic Eulerian Lagrangian methods for fluid-structure interactions with thermal fluctuations*, J. Comput. Phys., 230 (2011), pp. 2821–2837.

[22] W. Helfrich, *Elastic properties of lipid bilayers: Theory and possible experiments*, Z. Naturforsch. C, 28 (1973), pp. 693–703.

[23] J. M. Sullivan, *Curvatures of smooth and discrete surfaces*, in Discrete Differential Geometry, Oberwolfach Semin. 38, Birkhäuser, Basel, 2008, pp. 175–188.

[24] P. J. Atzberger, P. R. Kramer, and C. S. Peskin, *A stochastic immersed boundary method for fluid-structure dynamics at microscopic length scales*, J. Comput. Phys., 224 (2007), pp. 1255–1292.

[25] D. Devendran and C. S. Peskin, *An immersed boundary energy-based method for incompressible viscoelasticity*, J. Comput. Phys., 231 (2012), pp. 4613–4642.

[26] C. S. Peskin, *The Immersed Boundary Method.* III. *Energy Functions for the Representation of Immersed Elastic Boundaries and Materials*, handwritten lecture notes, http://www.math.nyu.edu/faculty/peskin/ib_lecture_notes/index.html (2007).

[27] P. J. Atzberger, S. Isaacson, and C. S. Peskin, *A microfluidic pumping mechanism driven by non-equilibrium osmotic effects*, Phys. D, 238 (2009), pp. 1168–1179.

[28] P. J. Atzberger and P. R. Kramer, *Theoretical framework for microscopic osmotic phenomena*, Phys. Rev. E, 75 (2007), 061125.

[29] M. Lai and C. S. Peskin, *An immersed boundary method with formal second-order accuracy and reduced numerical viscosity*, J. Comput. Phys., 160 (2000), pp. 705–719.

[30] C. R. Robinson and S. G. Sligar, *Hydrostatic and osmotic pressure as tools to study macromolecular recognition*, Methods Enzymol., 259 (1995), pp. 395–427.

[31] T. G. Fai, B. E. Griffith, Y. Mori, and C. S. Peskin, *Immersed boundary method for variable viscosity and variable density problems using fast constant-coefficient linear solvers I: Numerical method and results*, SIAM J. Sci. Comput., 35 (2013), pp. B1132–B1161.

[32] I. Doghri, *Mechanics of Deformable Solids: Linear, Nonlinear, Analytical and Computational Aspects*, Springer-Verlag, Berlin, 2000.

[33] P. J. ATZBERGER AND P. R. KRAMER, *Error analysis of a stochastic immersed boundary method incorporating thermal fluctuations*, Math. Comput. Simulation, 79 (2008), 379–408.

[34] J. PAN, S. T. NAGLE, AND J. F. NAGLE, *Temperature dependence of structure, bending rigidity, and bilayer interactions of dioleoylphosphatidylcholine bilayers*, Biophys. J., 94 (2008), pp. 117–124.

[35] S. E. FELLER AND R. W. PASTOR, *Constant surface tension simulations of lipid bilayers: The sensitivity of surface areas and compressibilities*, J. Chem. Phys., 111 (1999), pp. 1281–1287.

[36] D. P. TIELEMAN AND H. J. BERENDSEN, *Molecular dynamics simulations of a fully hydrated dipalmitoylphosphatidylcholine bilayer with different macroscopic boundary conditions and parameters*, J. Chem. Phys., 105 (1996), pp. 4871–4880.

[37] T. M. SQUIRES AND S. R. QUAKE, *Microfluidics: Fluid physics at the nanoliter scale*, Rev. Mod. Phys., 77 (2005), pp. 977–1026.

[38] J. H. VAN'T HOFF, *Stoechiom. Verwandtschaftsl.*, Z. Phys. Chem., 1 (1887), pp. 481–508.

[39] G. TABAK AND P. J. ATZBERGER, *Stochastic reductions for inertial fluid-structure interactions subject to thermal fluctuations*, SIAM J. Appl. Math., to appear.

[40] B. ALBERTS, A. JOHNSON, J. LEWIS, M. RAFF, K. ROBERTS, AND P. WALTER, *Molecular Biology of the Cell*, Garland Science, New York, 2002.

[41] S. A. WILLIAMS, J. B. BELL, AND A. L. GARCIA, *Algorithm refinement for fluctuating hydrodynamics*, Multiscale Model. Simul., 6 (2008), pp. 1256–1280.

[42] J. B. BELL, A. L. GARCIA, AND S. A. WILLIAMS, *Numerical methods for the stochastic Landau-Lifshitz Navier-Stokes equations*, Phys. Rev. E, 76 (2007), 016708.

[43] A. DONEV, J. B. BELL, A. L. GARCIA, AND B. J. ALDER, *A hybrid particle-continuum method for hydrodynamics of complex fluids*, Multiscale Model. Simul., 8 (2010), pp. 871–911.

[44] F. BALBOA USABIAGA, J. B. BELL, R. DELGADO-BUSCALIONI, A. DONEV, T. G. FAI, B. E. GRIFFITH, AND C. S. PESKIN, *Staggered schemes for fluctuating hydodynamics*, Multiscale Model. Simul., 10 (2012), pp. 1369–1408.

[45] E. M. LIFSHITZ AND L. P. PITAEVSKII, *Hydrodynamic fluctuations*, in Course of Theoretical Physics: Volume 9. Statistical Physics: Part 2, Theory of the Condensed State, Pergamon Press, Oxford, UK, 1980, pp. 360–384.

[46] L. D. LANDAU AND E. M. LIFSHITZ, *Viscous fluids*, in Course of Theoretical Physics: Volume 6. Fluid Mechanics, 2nd ed., Butterworth-Heinemann, Oxford, UK, 1987, pp. 44–94.

[47] P. J. ATZBERGER, *Incorporating shear into stochastic Eulerian-Lagrangian methods for rheological studies of complex fluids and soft materials*, Phys. D, 265 (2013), pp. 57–70.